CHARACTERIZATION OF TIN CATALYSTS

BY MÖSSBAUER SPECTROSCOPY

Final Report

by

G. Denes

Work on this project was conducted under the auspices of
Canada Centre for Mineral and Energy Technology,
Energy, Mines and Resources Canada

DSS FILE NUMBER	:	29ST.23440-5-9137
DSS CONTRACT SERIAL NUMBER	:	0ST85-00243
NRS SCIENTIFIC AUTHORITY	:	Dr. J. MONNIER

MICROMEDIA

CONCORDIA UNIVERSITY
DEPARTMENT OF CHEMISTRY
AND
LABORATORIES FOR INORGANIC MATERIALS
MONTREAL, QUEBEC

91 pp

INDEX

Summary....3

Résumé....5

Introduction....7

Experimental....11
1. Sample manipulation....11
2. Scanning electron microscopy....11
3. Powder X-ray diffraction....12
4. Mössbauer spectroscopy....12

Results and discussion....16
1. Scanning electron microscopy....16
2. Powder X-ray diffraction....17
2.1. Phase idendification....17
2.1.1. Introduction....18
2.1.2. Literature survey....18
2.1.3. Unused catalysts....18
2.1.3.1. Hydrous sodium titanate support....18
2.1.3.2. Tin ion exchanged catalysts....18
2.1.3.3. Tin coprecipitated catalysts (JM1)...20
2.1.4. Used catalysts....21
2.1.4.1. Tin ion exchanged catalysts 21
2.1.4.2. Tin coprecipitated catalysts (JM1)...23
2.2. Average particle size and degree of crystallinity....23
3. Mössbauer spectroscopy....26
3.1. Introduction and literature survey....26
3.2. Non calcined catalysts....27
3.3. Calcined catalysts....30
3.4. Used catalyst....31

Conclusion....34

Recommendations....36

References....39

Tables....41

Figures....73

SUMMARY

The goal of the research work presented in this report was to characterize some supported tin catalysts that have been prepared and tested in the Department of Energy, Mines and Resources. The main aim of the project was to characterize the tin metallic sites in the catalysts, which are believed to be responsible for their catalytic activity. ^{119}Sn Mössbauer spectroscopy has been used to probe the tin sites and has shown that most of the tin is present in the stannic form in a pseudo-octahedral coordination of oxygen atoms. Oxidation of tin(II) to tin(IV) during the ionic exchange is attributed to the air dissolved in the water solvent and is enhanced by hydrolysis. Some divalent tin is also observed in non-calcined catalysts but this is usually a minor component. This divalent tin is also surrounded by oxygen atoms (probably three or four) and shows a stereoactive lone pair of electrons on a non-bonding orbital with pronounced p character. After calcination in air at 400°C, all divalent tin has been oxidized to tin(IV). Used catalysts contain a major tin(IV) component similar to that before use. In addition there is a minor component of divalent tin which was identified as being SnS stannous sulfide. Powder X-ray diffraction experiments show in some cases no Bragg peak, and in others several peaks with considerable broadening. This is characteristic of the presence of small sized particles. Phase identification was not easy because of the large peak linewidth and thus poor resolution. The titanium-sodium oxygen supports give no Bragg peak while some SnO_2 is usually observed after ion exchange with tin. After calcination, TiO_2 and/or a $Ti_{1-x}Sn_xO_2$ solid solution become the major crystalline components, although it is also microcrystalline. Used catalysts also show Bragg peaks for SnS. Formation of SnS is explained by simultaneous reduction of tin(IV) from the solid solution and its sulfidation using the sulfur contained in coal. This results in the

decomposition of the solid solution and formation of TiO_2. The small particle size and absence of texture is confirmed by scanning electron microscopy which shows all samples are made of very small particles, which, in the case of calcined samples, are usually lumped together forming large blocks with no internal structure.

RESUME

Le but du travail de recherche présenté dans ce rapport était de caractériser des échantillons de catalyseurs d'étain supportés qui ont été préparés et testés au Département de l'Energie, Mines et Ressources. Le but principal du projet était la caractérisation des sites métalliques d'étain dans des catalyseurs qui sont soupçonnés d'être responsables de l'activité catalytique. La spectroscopie Mössbauer ^{119}Sn, utilisée pour l'étude des sites d'étain, a montré que la majeure partie de l'étain est présente sous forme stannique, l'étain(IV) étant entouré de six atomes d'oxygène formant une coordinance pseudooctaédrique. L'oxydation d'une grande quantité de l'étain(II) en étain(IV) au cours de l'échange ionique a été attribuée à l'oxygène dissous dans l'eau, l'oxydation étant activée par l'hydrolyse préalable de l'étain(II). Une faible quantité d'étain stanneux est aussi observée dans les catalyseurs non-calcinés. Cet étain stanneux est coordiné par de l'oxygène, probablement trois ou quatre, la paire libre d'électrons de l'étain(II) étant stéréoactive avec un caractère p important. Apres calcination à l'air à 400°C, tout l'étain(II) a été oxidé en étain(IV). La composante principale des catalyseurs calcinés est TiO_2 ou la solution solide $Ti_{1-x}Sn_xO_2$. Après utilisation, la majeure partie de l'étain des catalyseurs est toujours tétravalente, similaire à celui des catalyseurs non utilisés. De plus, une fraction plus faible d'étain(II) est aussi présente dans les catalyseurs usagés. Celle-ci a été identifiée comme étant le sulfure stanneux SnS. La formation de SnS a été expliquée par la réduction d'une partie de l'étain de la solution solide du degré +4 a +2, entrainant la décomposition de la solution solide et la libération de TiO_2, avec sulfidation simultanée de l'étain divalent formé, grâce au soufre contenu dans le charbon.

La diffraction de rayons X sur poudres montre une absence totale de pics de diffraction pour certains échantillons, tandis

que d'autres ont des pics de Bragg très fortement élargis. Ceci est caractéristique de la présence de particules de petite taille. L'élargissement considérable des pics de diffraction est à l'origine d'une résolution médiocre, ce qui a rendu difficile l'identification des phases cristallines présentes dans les échantillons. Les supports d'oxyde de titane et de sodium ne donnent aucun pic de Bragg alors que SnO_2 est observé après échange cationique avec l'étain. Après calcination, TiO_2 ou la solution solide $Ti_{1-x}Sn_xO_2$ devient le composant cristallin primordial bien qu'il soit aussi microcristallin. De plus, après utilisation des catalyseurs, les diagrammes de poudres contiennent des pics de Bragg de SnS. La présence de phases microcristallines et l'absence de texture et structure interne des catalyseurs est confirmée par les clichés de microscopie électronique à balayage qui montrent que les particules ont une dimension très petite et après calcination, il y a agglomération partielle de ces particules donnant des agglomérats de plus grande dimension qui toutefois n'ont toujours pas de structure interne.

INTRODUCTION

In catalytic reactions, it is essential to have as much information as possible regarding the nature and physical state of the catalysts used. Indeed, the efficiency and selectivity of catalysts can vary widely with parameters such as their chemical nature, their physical state (amorphous, bulk crystalline, deposited), the nature of the active sites, the coordination and oxidation state of the actif metals, the degree of crystallinity, the particle shape and size as well as the active surface area. The goal of this project was to use some of the solid state techniques, namely Mössbauer spectroscopy, X-ray diffraction and electron microscopy, to characterize some catalysts prepared by the Department of Energy, Mines and Resources, CANMET, Ottawa.

The anticipated shortage of oil and its capricious price has prompted intensive research about new sources of energy as well as use of cheapest or most convenient traditional energy sources. Research on coal liquefaction has been particulary active in countries rich in coal such as in Canada and Australia. Interesting results have been obtained using tin catalysts for hydroliquefaction of coal (1-3). In their effort of finding an attractive use of Canadian large deposits of both coals and heavy oil, the Energy Research Laboratories at CANMET have engaged in a research program based on the concept of coprocessing where coal is hydrogenated in the presence of bitumen or heavy oil of petroleum origin (4). Better conversions and higher quality liquids are obtained if catalysts are added to the liquid slurry (5). Recently, the Sandia National Laboratories of the US. Department of Energy developped new catalyst supports for coal hydrogenation utilizing metal-exchanged hydrous titanates (6,7). The samples investigated in the present project were prepared at CANMET Energy Research Laboratories in a similar manner to Dosch et al. (6,7). These samples are listed in Table I. For easy and short reference, each sample was assigned a code number JM1 to

JM19 as shown in Table I. The history of each sample is given on the diagram in fig.1.

The catalysts were prepared in CANMET laboratories as described in (8). The catalyst support was produced by reacting titanium(IV) isopropoxide with a solution of sodium hydroxide in methanol and precipitating the hydrous sodium titanate, $NaTi_2O_5H$, using a mixture of 10 wt % water in acetone. After washing and drying under vacuum, a white fluffy powder is obtained. Two batches of sodium hydrous titanate support (1st generation, JM13, and 2nd generation, JM14) were prepared and used to prepare the catalysts. In the next step, the tin exchanged hydrous titanate (MEHT) catalysts were obtained by ion exchange with sodium in an aqueous solution of stannous chloride dihydrate, $SnCl_2.2H_2O$. As shown in fig.1, MB-585 (JM10) and MB-586 (JM7) are obtained by ion exchange from the 1st generation support (JM13) while MB-599 (JM9) is obtained from the 2nd generation support (JM14), using the same technique. In one case, the support dissolved in the tin dichloride solution. Raising the pH by addition of ammonium hydroxide resulted in precipitation of a yellow solid (JM1) which strongly smelled ammonia even after washing and drying. As the titanium and tin solid species were simultaneously obtained on addition of ammonia, the solid obtained (JM1) was called "coprecipitated catalyst".

The last step of the preparation consisted in calcining the samples in air at 400°C for two hours. This gave the samples JM8, JM3, JM2, JM15, and JM19, which where obtained upon calcination of JM1, JM10, JM7, JM14, and JM9, respectively. JM15 is the 2nd generation support, not metal exchanged, heated in the same conditions.

The catalytic hydroprocessing tests have already been described (8). A mixture of catalyst, subbituminous coal and heavy oil heated at 410°C, is heated in an autoclave at 3.4MPa pressure, under continous hydrogen flow. After reaction, all the

liquids were drained, and the remaining solid (residue + catalyst) was washed with pentane, toluene and THF (tetrahydrofuran) to remove the oil, asphaltenes and prealphastenes. The THF insoluble solid consists mainly of the catalysts residue, the coke formed, as evidenced by petrographic analysis (8) and eventually, some unreacted coal. I was provided with four THF insoluble residues. JM6 (run #55 with MB-587), JM4 (run #54 with MB-586), JM11 and JM12 (runs #63 and #76, respectively, both with MB-599).

I received from CANMET fifteen samples, i.e. two titanate supports (JM13 and JM14), four non-calcined catalysts (JM1, JM10, JM7, and JM9), one calcined support (JM15), four calcined catalysts (JM8, JM3, JM2 and JM19) and four THF insoluble residues (JM6, JM4, JM11, and JM12).

In order to do a meaningful interpretation of my measurements, it was necessary to know the chemical composition of the samples. Furthermore, for the Mössbauer Spectroscopic measurements, it is useful to know in advance the tin content in the sample as the amount of sample used for the measurement depends on the amount of tin it contains. Indeed, an insufficient amount results in a very weak (and therefore inaccurate) spectrum or no spectrum at all. On the other hand, if the amount of sample is too large, line broadening (thus poor resolution) is observed, and in severe cases, the gamma count rate is too low, because of excessive non-resonant absorption, and results in a very weak spectrum. Table II gives relevant analytical results for several of the samples. When no results are given, they were not available to me. Two analytical techniques, viz. Inductive Coupled Plasma Argon Spectrometry (ICPAS) and Neutron Activation (NA) were used. Table II gives the results for Ti, Sn and Na. Sodium was the only significant contaminant. A low sodium level indicates that the ion exchange was complete, while for high contamination, possible formation of

sodium titanates or sodium stannates has to be considered. The results in Table II are given in weight % metal oxide (TiO_2, SnO_2 or Na_2O) for the ICAPS results and weight % metal (Ti, Sn or Na) for NA data. While the Ti and Sn results are similar for both techniques, as shown by similar Ti/Sn ratios, the sodium content is much higher for neutron activation than for ICAPS. This leads to Na/Sn and Na/Ti ratios which are about one order of magnitude higher for the neutron activation results. According to ICAPS analyses, the highest Na/Sn ratio is found for JM19 (Na/Sn=0.14). On the other hand, NA results indicate Na/Sn ratios are close to 0.5 for JM2 and JM3, over 1 for JM19 and equal 5 for JM8. If these high ratios are to be believed, formation of large amounts of sodium stannates is possible. On the other hand, if sodium titanates were formed, it would be only in small amounts as the highest Na/Ti neutron activation result is Na/Ti=0.22 for JM19, while the ICAPS values are negligible. As a consequence of the analytical results available to me, I concluded that sodium may be present in sufficient quantity to form large amounts of sodium stannates and small amounts of sodium titanates. X-ray diffraction and Mössbauer data were checked for the formation of such species. Table III identifies the techniques used in this project for the study of the fifteen samples. All tin-containing samples, i.e. all catalysts, but not the supports, were studied by Mössbauer spectroscopy. X-ray powder diffraction was performed on all samples. Scanning electron microscopy was used for the supports and all non-used catalysts (non-calcined and calcined). No electron micrographs were taken for the THF insolubles because it would be hard to see the used catalysts which were intimately mixed with a large amount of coke or unreacted coal. In the following sections, I give: (i) the experimental techniques (equipment, experimental proceduces), (ii) the results of the analyses performed and a dicussion of the results, (iii) the general conclusions and in (iv) the recommendations based on my observations.

EXPERIMENTAL

1. SAMPLE MANIPULATION

All samples were fine powders. The color of the catalysts was yellow, light yellow or white while the THF insoluble residues were black, as listed in Table IV. All samples seemed unreactive to air at room temperature and therefore were handled in air with no special precaution.

2. SCANNING ELECTRON MICROSCOPY

The samples for electron microscopy were ground and dried in air at ca. 120°C overnight to remove adsorbed water. Then they were stored in a dessicator. A small amount of each sample was sprinkled on an electron microscopy 0.5 inch diameter aluminum stub to which a sticky tab had previously been applied. The excess powder was removed by shaking and blowing a gentle breeze of nitrogen on the stub. As the samples are obviously not good electrical conductors, gold coating was applied in a vacuum deposition system to avoid electric charge build-up during electron irradiation, which would cause focusing problems. The micrographs were taken using a polaroid camera on a Hitachi S-520 scanning electron microscope operating with the filament energized at 15kV. The electron microscope has a feature allowing to split the screen (and thus the micrographs) by the middle in order to have on the same picture two different amplifications of the same area of the sample. I used this useful feature for most of the micrographs taken in the present work. The magnification given at the bottom of the picture corresponds to the upper half picture (for example: X 5.00K means "magnification 5,000) while the magnification of the lower half is a multiple integer of that of the upper half. The multiple, given by a code letter A,B or C at the bottom right corner of the micrograph is 2 (letter A), 5 (letter B) or 10 (letter C). A distance scale is also shown at the bottom of the picture. The white-sided rectangular box in the upper half of the picture corresponds to the area that is

shown in the lower half after further magnification by 2,5 or 10.

3. POWDER X-RAY DIFFRACTION

All X-ray diffraction patterns were run on finely ground powders which were packed in a plexiglass holder, using a glass microscope slide, then mounted at the center of the goniometer a Picker X-ray diffractometer/X-ray fluorescence spectrometer dual instrument. The K-alpha radiation of Cu was used, the K-beta line being filtred by a Ni foil filter. The scans were run at a speed of 0.5^0 (θ) $.min^{-1}$ in the range $3\text{-}40^0$ (θ). Tests at lower speeds did not provide higher accuracy because of large linewidth and strong peak overlapping. The powder patterns were recorded on chart paper as the intensity of diffracted X-ray beam versus the angle (θ) between the surface of the sample and the incident X-ray beam. An alpha-SnF_2 standard sample was run before and after each pattern for checking the line positions. This was also used as standard for linewidth, for correcting the observed line broadening from the instrumental broadening in the determination of average particle size.

4. MÖSSBAUER SPECTROSCOPY

Mössbauer spectra were recorded on a Mössbauer spectrometer that I recently set up at Concordia University (9). The 23.875 KeV Mössbauer gamma-ray line was obtained using a 15mCi $Ca^{119m}SnO_3$ source purchased from Amersham. The Doppler velocity was provided by an Elscint driving system including a MVT-4 velocity transducer, a MFG-N-5 function generator and a MDF-N-5 driver generator, powered from a EG&G ORTEC NIM-BIN, and operating in the triangle mode. The 25.04 and 25.27KeV X-ray lines were removed using a 0.1mm thick palladium foil filter. The gamma-rays were recorded using a Harshaw power supply and Na(Tl)I scintillation counter operating at 900V. The samples were finely ground powders, generally in the amount necessary to give 10mg $Sn.cm^{-2}$, based on the analytical data of Table II.

This amount is sufficient to give a strong resonant gamma-ray absorption, yet well below saturation level. In some cases (JM1,JM7 and JM19), this amount was found to be insufficient and it was increased. In the case of JM16, as there was not a sufficient amount of the sample to have 10mg $Sn.cm^{-2}$, the whole sample was used, corresponding to 6.6mg $Sn.cm^{-2}$, which was enough to give a good Mössbauer spectrum. When no analytical data was available (JM9 and JM10), the amount to be used was determined by comparison with similar samples, which gave good results.

Neat samples were loaded into polytetrafluoroethylene (teflon) or aluminum holders with a tightly fitting screw cap . Both sample holder and cap have a thin window of $3cm^2$ area. The sample holders are fitted inside a 1cm thick wall brass cylinder which is fitted at the top a 2cm thick wall lead cylinder for shielding purposes. The source was vibrated inside the lead cylinder, along the cylinder axis. The lead cylinder, with the brass holder containing the teflon sample holder mounted on its top, was mounted on the top of the velocity transducer, and the whole thing was resting on the vibration-free table, in the vertical position. The source and absorber must be protected against all sources of external vibrations such as pumps, fans from electrical appliances, etc..., so common in research laboratories. Indeed, gamma-ray modulation is done by Doppler effect, i.e. by moving the source relative to the absorber. The Doppler modulation, in the case of ^{119}Sn Mössbauer spectroscopy, is in the range -8 to +8$mm.s^{-1}$ source velocity, which corresponds to common frequencies of vibrations of pumps and fans. External sources of vibration would therefore distort the gamma-ray modulation, resulting in significant line broadening and thus serious loss of resolution. Protection against external vibrations is provided by having the transducer, thus the source and the absorber on the vibration-free table. The table is a large aluminum plate ($310x105x2cm^3$) sustained by six legs attached to ciment blocks which are immersed in three sand boxes

which are protected from the floor by a thick rubber sheet which provides a damping of the vibrations. The vibrations not stoppped by the rubber are absorbed by the sand. All electrical parts of the spectrometer that have a fan for cooling and therefore are sources of vibrations, i.e. the multichannel analyzer, the NIM-BIN and the high voltage power supply, are mounted on a four-wheeled rack resting on the floor, with no physical connections to the vibration-free parts, except electrical cables. This arrangement works well as no significant instrumental line broadening was detected. The source to detector distance was maintained at 16cm . This, combined with the small amplitude of vibration of the source provided by a transducer frequency of 22Hz, gives spectra free of cosine broadening.

Both source and absorber were maintained at room temperature for all measurements. This provides strong spectra as the recoil-free fraction of tin oxides is high for both the divalent and tetravalent oxidation states (10). The Doppler velocity modulation was maintained in the range of -8 to +8mm.s^{-1} for studying both di- and tetravalent tin, while a velocity range of -2.5 to +2.5mm.s^{-1} was used for a detailed study of the tin(IV) signal.

The signal from the scintillation counter is fed into a Tracor Northern 7200 multichannel analyzer were it is amplified by a built-in linear amplifier. Then the Mössbauer gamma-ray line is isolated in the built-in single channel analyzer. Finally, the signal is stored in a quarter (512 channels) of the 2K memory multichannel analyzer. The multichannel analyzer is operated in the multiscaling mode with the dwell time being controlled by the Elscint driving system in order to have synchronization of the source motion with the multichannel analyzer channel scanning. The spectrum is accumulated (source moving towards absorber) in the first 256 channels of the selected quarter of the memory and its mirror image (source moving away from

absorber) in the next 256 channels. When the counting statistics is estimated to be sufficiently good, (usually after 500,000 to 1,000,000 counts/ channel have been accumulated, data acquisition is stopped and the data are transferred to an IBM compatible personal computer and stored on a diskette. Relevant experimental parameters for the Mössbauer runs are given in Table IV.

The data were calibrated using a $CaSnO_3$ and an alpha-SnF_2 standard absorbers as described in (9). The line position for $CaSnO_3$ at room temperature was taken as reference of isomer shift.

RESULTS AND DISCUSSION

1. SCANNING ELECTRON MICROSCOPY

The SEM micrographs for samples JM1, JM2, JM3, JM7, JM8, JM9, JM10, JM13, JM14, and JM15 are shown on figs. 2 to 11. Usually two magnifications were used for each sample, in order to show the particle shape and their internal structure. The highest magnification used was usually the highest that could be obtained. For even higher magnifications, the pictures could not be focused properly because of the absence of internal structure of the particles.

Vacuum dried hydrous sodium titanate supports (JM13 and JM14) are white fluffy powders with no microscopic structure. The first generation support (JM13) is made of loosely bound very small particles, of which size is much too small to be clearly resolved on this type of microscope (fig 9). The second generation support consists of larger particles, some as large as ca. 2μm diameter however these particles show no internal structure and are probably made of an agglomeration of much smaller amorphous particles (JM14).

Metal exchanged fresh catalysts, i.e. before calcination (JM1, JM7, JM9 and JM10) contain a mixture of larger blocks (10-50μm) and smaller particles. All these blocks are irregular in shape, showing no evidence of crystallization. In addition magnification of these blocks show they are agglomerates of much smaller particles and they have no internal structure. Therefore, ion exchange results in macroscopic agglomeration of particles but seems not to lead to much internal reorganization, although there is a reorganization at the atomic level.

After calcination, (catalysts JM2, JM3 and JM8), no much change is observed, i.e. the samples are still mixtures of large blocks (30-60μm) irregularly shaped, mixed with smaller blocks (a few μm's diameter) and very small particles (fig. 3, 4 and 6). The absence of internal structure of the blocks is again

confirmed at higher magnifications, showing that all these blocks are made of much smaller particles. This shows that the temperature of calcination was not high enough to make the crystallites grow sufficiently big to be resolved on the micrographs, and it was also too low to sinter the samples. One can therefore conclude that in all these catalysts, the average crystallite size is at most a few hundred Å in diameter. Calcination of the sodium hydrous titanate not exchanged by tin, gives a significant agglomeration of the material (JMI5, obtained by calcination of JM14). Indeed, the JM14 support, which is made of particles of diameter 2μm or less before calcination, shows many porous lumps with a diameter of 20-50 μm (JM15) after calcination. However, these lumps again have no internal structure, showing that the crystallite size is much smaller.

2. POWDER X-RAY DIFFRACTION

2.1. Phase identifaction

2.1.1. Introduction

All samples were either amorphous or microcrystalline, and thus gave broad lines sometimes difficult to distinguish from the background noise. As a result of the low resolution, phase identification and determination of cell parameters were difficult, due to the strong peak overlapping, the difficulty of measuring Bragg angles and the low signal/background ratio. However, useful information, such as phase identification, estimates of cell parameters and average particle dimension was extracted from the X-ray powder pattern of most of the samples. The low degree of crystallinity is not surprising for these samples prepared using the precipitation techniques and agrees well with the electron microscopy results.

2.1.2. Literature survey

In order to identify the crystalline phases present in the catalysts, an extensive survey of the literature on relevant

possible compounds or by-products was done. The results of this survey, taken from the ASTM X-ray powder file and from the original publications when available, are given in Table V. Based on the preparative techniques the following compounds were considered: titanium(IV) oxides, sodium titanates(IV), all tin oxides, sodium stannates and for all of the above, all their hydroxides and hydrates. In addition, for the used catalysts, sulfidation of titanium and tin were considered with possible reduction of tin to the metallic state. For all tin compounds, all oxidation states were considered possible, i.e., the metal, +II, +IV and mixed oxidation state compounds. No data on tin titanates(IV) or tin thiotitanates(IV) was found, thus it was assumed no such compound is presently known. A list of Bragg peaks for all possible compounds found in the literature was made and used for comparison with the experimental powder patterns shown in Table VI.

2.1.3. Unused catalysts

2.1.3.1. Hydrous sodium titanate supports

The powder pattern of both hydrous sodium titanate supports consists of a featureless baseline with no Bragg peak [figs. 12(a), 13(a), 14(a), 15(a) and Table VI], showing that these samples are amorphous or microcrystalline with a particle size smaller than 50Å diameter. These results are in agreement with the absence of internal structure of the small lumps observed by electron microscopy and corroborate the findings of Dosch et al. (6, 7).

2.1.3.2. Tin ion exchanged catalysts

The non-calcined catalysts obtained by ion-exchange (JM7, JM9 and JM10) give very broad signals barely distinguishable from background fluctuations [figs. 12(b), 13(b), 14(b) and Table VI], which show the presence of microcrystalline stannic oxide SnO_2, in the rutile form, made of very small particles.

Calcination of these samples leads to a significant increase in the crystallinity and particle size, which however stay very small such that individual crystallites cannot be resolved by the electron microscope used in this study. Calcination of JM7, JM9, and JM10 gives the JM2, JM19, and JM3 samples respectively [figs. 12(c), 13(c), 14(c) and Table VI]. Comparison of figs. 12(c), 13(c) and 14(c) shows that the powder patterns obtained are quite different. The main crystalline component of calcined MB-586 (JM2) is the anatase polymorph of TiO_2 with a significant amount of SnO_2 in the rutile polymorph and probably a smaller amount of TiO_2 in the rutile form. One Bragg peak, indicated by an X on fig. 12(c), could not be identified as any known compound of tin or titanium(IV) that could have been formed in this reaction. This peak has been attributed to a $Ti_{1-x}Sn_xO_2$ rutile type solid solution as explained for the JM19 sample. The powder pattern of calcined MB-587 (JM19) looks simpler, i.e. made of a lower number of Bragg peaks [fig 13(c)] which however are broader. The second of these peaks corresponds to the undentified peak of JM2 marked by an X [fig. 12(c)]. This simple powder pattern could not be attributed to any oxide (anhydrous or hydrated) of tin or titanium(IV) (with or without sodium) listed on Table V. Therefore JM19 does not contain TiO_2 anatase, TiO_2 or SnO_2 as JM2. However, because of the simplicity of the pattern, I was able to index it in a tetragonal cell with the cell parameters being a = 4.643Å and c = 3.100Å. Identification of this new tetragonal material becomes easy once one notices that each of its (hkl) Bragg peak is located between the corresponding Bragg peaks of TiO_2 rutile and SnO_2 rutile, which seems to indicate that the compound formed is a solid solution $Ti_{1-x}Sn_xO_2$ crystallizing in the rutile form. The unidentified peak on JM2 [fig. 12 (c)] corresponds to the (101) peak of $Ti_{1-x}Sn_xO_2$, indicating that a small amount of mixed tin-titanium oxide solid solution had also formed in JM2. Close examination of fig. 12(c) shows that the (110) peak of the tin titanium oxide

solid solution is also visible, between the (110) peaks of SnO_2 rutile and TiO_2 rutile, corroborating the presence of a small amount of solid solution. The unit cell parameters of the $Ti_{1-x}Sn_xO_2$ rutile phase are compared to those the rutile forms of SnO_2 and TiO_2 in the table below:

Unit-cell parameters	TiO_2	$Ti_{1-x}Sn_xO_2$	SnO_2
a (Å)	4.594	4.643	4.738
c (Å)	2.958	3.100	3.188
V ($Å^3$)	62.43	66.83	71.51

Based on these findings, a close examination of the powder patterns of the non-calcined ion-exchanged catalysts (JM7, JM9 and JM10) reveals that these could as well be formed of the $Ti_{1-x}Sn_xO_2$ solution instead of SnO_2 and TiO_2 in the rutile form. However, their very low crystallinity does not make possible a unambiguous identification of the extremely broad Bragg peaks observed.

The powder pattern of calcined MB-585 (JM3) is very similar to that of calcined MB-586 (JM2), i.e. it is made of a large amount of TiO_2 anatase, the $Ti_{1-x}Sn_xO_2$ rutile type solid solution as in JM2, with some SnO_2 rutile and probably some TiO_2 rutile. However there seems to be a larger amount of TiO_2 anatase with, as a result, less TiO_2 rutile. The amount of SnO_2 is also smaller.

2.1.3.3. <u>Tin coprecipitated catalyst</u> (JM1)

As indicated in the introduction, in one case, the JM13 hydrous sodium titanate support dissolved upon addition of the $SnCl_2.2H_2O$ aqueous solution. As the pH was raised by addition of NH_4OH, the tin and titanium species coprecipitated to give the JM1 coprecipitated catalyst. The results of the X-ray diffraction analysis are shown on fig. 15. The powder pattern of the non-calcined coprecipitated catalyst (JM1) contrasts sharply

with that of its ion-exchanged counterpart as it shows a few sharp peak indicative of a much larger grain size [fig. 15(b)]. The first peak at $\theta = 11.58^0$ could not be assigned. The rest of the peaks could be assigned to a mixture of Sn_3O_4 and $Sn_5O_3(OH)_4$. However, it is very likely these are not the real phases present in the sample for the following reasons:

- several strong peaks of Sn_3O_4 and of $Sn_5O_3(OH)_4$ are not observed. If the sample contained these species, all their strong peaks should be observed.
- the first peak, being not accounted neither by Sn_3O_4 nor $Sn_4O_3(OH)_4$, belongs to another crystalline phase. This other species must have other peaks that should be observed, however as there is no other unaccounted peak, all of them would have to overlap with the peaks of Sn_3O_4 and $Sn_5O_3(OH)_4$. Such a coincidence is highly unlikely.

Therefore one can safely conclude that it is very likely the JM1 non-calcined coprecipitated catalyst contains neither Sn_3O_4 nor $Sn_5O_3(OH)_4$. It contains one or more crystalline phases that could not be identified. This conclusion is corroborated by Mössbauer spectroscopy.

After calcination the coprecipitated catalyst (JM8) gives a powder pattern that is different of the pattern before calcination. Most of the peaks could be accounted for by TiO_2 in the anatase form. However, the two peaks labelled X on fig. 15(c) could not be identified; the first of them was also present before calcination [fig. 15(b)]. All the other peaks observed before calcination have disappeared, indicating that they belonged to a species thermally unstable in air at 400°C, possibly a hydrate or an ammonium-containing compound.

2.1.4. Used catalysts

2.1.4.1. Tin ion-exchanged catalysts

Some significant changes in the X-ray diffraction pattern occur during the catalytic reaction, as shown on

fig. 12(d), 13(d) and 13(e). The first observation is that the powder pattern is more complex. The new peaks can be accounted for by the formation of SnS and possibly a small amount of metallic tin (beta-Sn). Partial reduction of tin is not surprising as the reaction mixture is a highly reducing medium (elemental carbon and hydrogen under pressure). Sulphidation could be explained by the presence of sulphur (2.3 wt %) in the feed slurry. As no tin(IV) sulphide (SnS_2) or mixed oxidation state tin(II)-tin(IV) sulphide (Sn_2S_3, i.e. Sn(II)Sn(IV)S_3, and Sn_3S_4, i.e. Sn(II)$_2$Sn(IV)S_4 are known), it is possible that only tin(II) already present in the catalyst (although this would be surprising after 2 hours calcination at 400°C in air) is sulphided, or reduction of tin(IV) to tin(II), then sulphidation, occur in the same reaction process during the catalytic reaction.

For MB-599 (fig. 13), another important feature observed after the catalyst has been used (JM11 and JM12) is the formation of TiO_2 anatase when none was present in the catalyst before use (JM19). At the same time, the amount of rutile solid solution $Ti_{1-x}Sn_xO_2$ seems to have significantly decreased. Such a behaviour can be explained based on the reduction of the $Ti_{1-x}Sn_xO_2$ solid solution by hydrogen (reaction I) or carbon (reaction II) and simultaneous sulphidation of the divalent tin to form SnS. This reaction releases TiO_2, which is found to crystallize in the anatase polymorph.

(I) $xS^{2-} + Ti_{1-x}Sn_xO_2 + 2xH_2 \longrightarrow (1-x)TiO_2 + 2xH_2O + xSnS + 2xe^-$
rutile anatase

(II) $xS^{2-} + Ti_{1-x}Sn_xO_2 + 2xC \longrightarrow (1-x)TiO_2 + 2xCO + xSnS + 2xe^-$
rutile anatase

No sulphidation and/or reduction of titanium was observed. No significant difference was observed between JM11 and JM12,

showing that calcination has no significant effect on the results.

2.1.2.2. **Tin coprecipitated catalyst** (JM6).

As shown on fig. 15d, the powder pattern after use of the catalyst is more complex. Formation of SnS or beta-Sn is again possible although it is difficult to be certain about it as their major peak would occur at about the same θ angle that the first unidentified peak of the unused catalyst which may still be present as is the second. In addition two new weak peaks at θ= 14.25 and 14.70 are also observed and cannot be accounted for.

Furthermore there is considerable complications of the TiO_2 Bragg peaks (JM6) when the only phase of TiO_2 observed on the unused catalyst is anatase, the used catalyst seems to be best understood as a mixture of the three most common forms of TiO_2, i.e. anatase, rutile and brookite, with in addition at least one unknown crystalline phase, and possibly some SnS and/or Sn. No SnO_2 is observed before or after catalytic reaction. The (110) peak of SnO_2 rutile could be present at c.a. 13.30° (θ) but the peak of relative intensity 90 at 17.06° (θ) being not observed rules out the presence of crystalline SnO_2 rutile in the JM6 used catalyst.

2.2. **Average particle size and degree of crystallinity.**

Absence of Bragg peaks or broadened peaks for all samples, except JM1 is indicative of a low degree of crystallinity. This is not surprising as precipitation techniques often lead to the formation of gels, amorphous or poorly crystalline solids.

The average particle size of the crystallites was determined using Scherrer formula (11).

$$t(\text{Å}) = (0.9\,\lambda)/(B.\cos\theta)$$

where t is the average particle size in Å

λ is the wavelength of the radiation in Å

θ is the Bragg angle for the Bragg peak used

B is the broadening at half height due to the small size of the particles.

Correction for instrumental line broadening was done using Warren's method (11):

$$B^2 = B_M^2 - B_S^2$$

where B is the same as in Scherrer formula.

B_M is the experimental linewidth for the sample.

B_S is the experimental linewidth for a well crystalline standard material (particle diameter > 1,000Å). Alpha-SnF_2 was used as standard for zeroshift in line position and for instrumental line broadening correction as its line positions are well known and it is well crystalline, thus exhibits no line broadening due to microcrystallinity.

Table VI gives the list Bragg peaks for each sample. The linewidth at half height is given when measurable. The main Bragg peak for the alpha-SnF_2 standard is also given as a check for possible lineshift and as instrumental line broadening standard. The standard sample was ran just before and just after each sample. The results for alpha-SnF_2 show the reproducibility of both line position and line shift. The results presented in Table VIII show that most of the samples exhibit considerable broadening and are thefore microcrystalline.

Total absence of Bragg peaks for the supports (JM13 and JM14) shows the particle diameter is smaller than 50Å. It is also possible than these particles are amorphous. Microcrystalline or amorphous materials are often obtained in reactions resulting in fast precipitation. Therefore this result is not surprising. The ion exchanged tin catalysts prior to calcination (JM7, JM9 and JM10) are made of SnO_2 or $Ti_{1-x}Sn_xO_2$ rutile phase in the microcrystalline form. Considerable line broadening (5 to 10 times as broad as the lines for the standard) is indicative of small sized particles. Only a rough estimate of the particle size can be proposed as the lines are

hardly distinguishable from the background and therefore measurement of the linewidth is extremely difficult. In addition, overlapping of broad peaks could give an envelope much broader than its individual components. The particle diameter has been estimated to be in the range 50-100Å or close to it.

Calcination of the ion exchanged catalysts (JM2, JM3 and JM19) results in the formation of TiO_2 in the anatase polymorph together with SnO_2, TiO_2 and/or $Ti_{1-x}Sn_xO_2$, all three in the rutile form, except JM19 that shows only $Ti_{1-x}Sn_xO_2$. The anatase peaks are stronger, narrower, and show less overlapping with other peaks such that a higher precision on the average particle size can be obtained. In all three cases, it was 300-330Å. The rutile-type phase shows broader lines with more overlapping. The average particle diameter was calculated to be around 120Å for JM3 while it could not be measured for JM2 because of too much overlapping. However, it is clear that it is in the range 150-200Å.

Used catalysts show results comparable to the unused calcined catalysts with similar particle dimensions i.e. 330 Å for anatase, 100-150Å for the rutile phases. The lines for SnS were too weak to allow a meaningful measurement of the linewidth. However, it is likely it is also present in the microcrystalline form. The coprecipitated catalyst (JM1), on the contrary, shows little broadening, if any, which indicates much larger particle size (around 1,000Å). After calcination, the unknown species still show large particles (around 800 Å), while the anatase TiO_2 that has formed upon calcination has particles of about 140Å diameter, i.e. about half the value for the calcined ion-exchanged catalysts. The peaks at 15.77 and 22.60° after use of the catalysts, that could be SnS or beta-Sn or the unknown phase observed before use, are stronger and narrower, giving particle diameters of about 800 and 1500Å respectively, which suggest they are due to the unknown phase and not to beta-Sn or SnS.

It is obvious from this study that all ion-exchanged

samples are microcrystalline, with the support having so small particle dimension that it precludes detection by the diffraction techniques. Ion exchange leads to a microcrystalline rutile type (or mixtures of them) with small particle size (usually 50-100Å). Calcination results in the formation of TiO_2 anatase with 300-340Å particle dimension, but the calcination temperature is insufficient to bring about significant crystallite growth of the rutile phase, which shows particle dimensions of 100-130 Å. Calcination of the non-exchanged JM14 support in the same conditions (400°C for 2 hours in air) is also not sufficient to recrystallize or grow the crystallites of the support as the resulting product (JM15) still shows no Bragg peak. Little change in particle size is observed after use of the catalysts. The small particle size is not surprising as the catalysts are obtained by precipitation reaction. However, the coprecipitated catalyst is different as unknown compounds that are not microcrystalline are observed. The X-ray results corroborate the electron micrographs as they show the samples are made of very small particles. This shows that the smaller particles observed in electron microscopy (1-2μm) are, indeed, agglomerates of a large number (about 10^{10}) of much smaller size particles (diameter about 1,000 times smaller), which explain the irregular shape and absence of internal structure of the aggregates.

3. MÖSSBAUER SPECTROSCOPY

3.1. Introduction and literature survey

The Mössbauer technique uses the ^{119}Sn isotope for probing local electric and magnetic conditions at the tin sites. Even minute changes in the electrical or magnetic environment of tin will slightly shift and/or split the nuclear energy levels and therefore give rise to changes in the Mössbauer spectrum (line-shift and/or splitting). Mössbauer spectroscopy is used as an analytical tool to evaluate the tin species contained in the catalysts and estimate their relative quantities. The tin

species can be identified from their isomer shift (line shift) and quadrupole splitting (line splitting) provided the Mössbauer data for the corresponding compounds have been published. As tin is diamagnetic in all stable oxidation states (0, +2 and +4), no magnetic hyperfine splitting is observed unless tin is embedded in a magnetically ordered structure (transferred field) or if an external field is applied. The isomer shift is characteristic of the s electron density at tin, such as the oxidation state (which is easily extracted from the spectra), as well as the nature of the ligands and often a good idea of the tin coordination is obtained. The quadrupole splitting, due to the interaction between the quadrupole moment of the tin nucleus in the first excited state and the electric field gradient (e.f.g.) acting at the tin nucleus, is therefore a function of the magnitude and symmetry of the e.f.g., i.e. the site distortion at tin and the participation of p and d orbitals in bonding.

Mössbauer parameters for relevant tin compounds are shown on Table IX and are compared to the results for the samples (Table X). The percentage contribution of each tin species to the total spectrum is given, as well as the assignment of the tin sites and tin oxidation state. Of course, the sodium hydrous titanate supports (JM13, JM14 and JM15) could not be studied by Mössbauer spectroscopy as they do not contain tin.

3.2. Non-calcined catalysts

All non-calcined catalysts (JM1, JM7, JM9 and JM10) contain two kinds of tin species, the major part being tetravalent and the minor part divalent. The exact ratios Sn(II)/total Sn and Sn(IV)/total Sn cannot be determined precisely because their recoil-free fraction is likely to be different, which results in different constants of proportionality between the contribution of each species to the the total signal and their actual abundance in the sample. Therefore, the proposed ratios are estimates and should not be

taken as absolute values (see paragraph on recommendations).

The coprecipitated catalyst (JM1) and the ion-exchanged catalysts (JM7 and JM10) prepared using the first generation support (JM13) contain 5% (for JM1 and JM7) and 10% (for JM10) divalent tin, thus respectively 95% and 90% tetravalent tin. On the other hand, JM9, prepared from the second generation catalyst (JM14) contains 25% Sn(II) and 75% Sn(IV). As the ion exchange is done using $SnCl_2.2H_2O$, i.e. divalent tin, a large amount of tin is oxidized in the ion exchange process. However, a larger amount of Sn(II) is found in JM9 than in the others. This indicates that the oxidizing conditions were milder in that case. This could be due, either to the support which is not the same (JM14, second generation support), to the conditions or medium in the ion exchange process which could have been slightly different, or to a shorter exposure to the oxidizing conditions, for example if the ion exchange was carried out faster. It is well known that divalent tin(II) spontaneously oxidizes to tin(IV) in aqueous solutions (12), such that a shorter period of time in aqueous solution could be the reason for the presence of a larger amount of Sn(II) in JM9 (25% instead of 5-10%). Tin(II) is also suspected to oxidize via a hydrolysis process, using oxygen dissolved in the water solvent, such that a lower pH and degassing the water will slow down the oxidation of tin. The relative amount of tin(II) in the ion exchanged non-calcined catalysts is compared to the preparative conditions in Table XI. JM7, which was prepared at the highest pH (2.8) and in non-degassed water, contains the smallest amount of Sn(II) (5%). At a pH slightly lower (2.4) and for degassed water (JM10), 10% of Sn(II) is observed. If the pH is significantly lower (1.825 for JM9), and again using degassed water, the amount of Sn(II) is much higher (25%). This trend agrees with our present knowledge on the oxidation of divalent tin in aqueous solution, i.e., it is slower in strongly acidic solution and the oxygen dissolved in water is, at least in part, responsible for the oxidation to

tetravalent tin. Of course, it is also a function of time, i.e., the amount of tin(IV) increases with time (12). However, in this case, the longest time (105 minutes for JM9) results in the largest amount of tin(II) because the other conditions (pH and degassing) are more efficient to prevent (or slow down) oxidation, and therefore partly cancel the time effect. Some effect of the nature of the support is also possible, but the lack of structural information regarding them precludes any conclusion in this regard.

The tin(IV) Mössbauer parameters (isomer shift close to zero, small quadrupole splitting) are characteristic of Sn(IV) in a pseudo-octahedral coordination of oxygen atoms. These oxygen atoms can be chemically different, i.e. they can be bridging oxygen atoms (between two Sn or a Sn and a Ti), OH^- hydroxyl ions or H_2O water molecules. Therefore the coordination of tin(IV) is similar to that of Sn in SnO_2 cassiterite (13) however the oxygen atoms surrounding Sn can be of different nature as in $SnO_2.xH_2O$ which has been observed in tin-treated coals (14).

The divalent tin gives a well resolved doublet at highly positive isomer shift ($\delta \simeq 3$ mm.s^{-1}, Δ = 1.6 to 1.9 mm.s^{-1}). This is characteristic of Sn(II), with its non-bonding electron lone pair being stereoactive. This results in a strongly distorted environment and a lower coordination of tin (II). Such structural consequences of the stereoactivity of main group elements non-bonded pair has been studied by Galy et al. (15) and Brown (16), based on the VSEPR theory of Gillespie and Nyholm (17) and applied to divalent tin by Denes et al. (18). The tin(II) non-bonded pair, when stereoactive, contains much p character, which results in a strong electric field gradient at tin, giving rise to large quadrupole splittings (Δ >1.50mm.s^{-1}) (19). Coordinations such as distorted SnX_3E tetrahedra and SnX_4E trigonal bipyramids (X= F or O, E= lone pair) are commonly encountered (18 & 20). The divalent tin species in these catalysts could not be identified with any of the tin(II) oxides

or hydroxides or their hydrates already reported in the literature and given in Table IX, such as SnO, SnO.yH2O or Sn5O3(OH)4 or those of mixed oxidation tin oxides such as Sn2O3 or Sn3O4. As the tin(II) species present in the catalysts give no visible X-ray diffraction pattern, they are amorphous or microcrystalline with particle diameters not larger than 50Å. This, combined with the fact that they are mixed with other phases (hydrated tin (IV) and titanium (IV) oxides) precludes further identification. The fact that the tin(II) Mössbauer parameters are different from those of Sn5O3(OH)4 is a further prove of the non-existence of this compound in the JM1 coprecipitated catalyst despite accidental coincidence of several X-ray Bragg peaks.

In addition to variable ratios tin(II)/total tin, one can see that the isomer shift and quadrupole splitting changes significantly from one sample to another, indicating a different local arrangement of ligands around tin(II) and thus different coordination. These fluctuations are probably correlated to small changes in the conditions of preparation.

Another interesting Mössbauer result is that the coprecipitated (JM1) and ion-exchanged catalysts (JM7 and JM10) prepared using the first generation support (JM13) give almost identical Mössbauer spectra. This indicates that tin species they contain are likely to be similar. Therefore, difference in X-ray powder patterns is probably due to a titanium-containing compound. Unfortunately this cannot be studied by Mössbauer spectroscopy as titanium has no Mössbauer isotope.

3.3. Calcined catalysts (JM2, JM3, JM8 and JM19).

All calcined catalysts show only one peak at about zero velocity, characteristics of tetravalent tin in an octahedral coordination of oxygen atoms. In most of the samples, the peak is slightly broadened, indicating a distortion from regular octahedral symmetry. This is not surprising as divalent tin,

although usually fairly stable at ambient temperature, is known to undergo rapid oxidation to tin(IV) when heated in an oxidizing atmosphere. Therefore, calcination for 2 hours at 400°C in air could be expected to yield tetravalent tin only. The broadening of the Mössbauer line can be explained, based on the X-ray diffraction results that the tin(IV) species after calcination is SnO_2 rutile or a $Ti_{1-x}Sn_xO_2$ solid solution which crystallizes also in the rutile form. Indeed, it is well known that the metal M in the MX_2 rutile structural type, is surrounded by six X atoms at the corners of a distorted octahedron, resulting in the presence of a non-negligible electric field gradient a tin, giving rise to a small quadrupole splitting (0.10 to 0.60mm.s^{-1}). In the calcined catalysts, most if not all of the water present in the catalysts has been removed, therefore all oxygen atoms are probably bridging (between Sn and Ti). The slight difference in isomer shift and quadrupole splitting between the samples reflects small differences in bonding, and coordination of tin and may be due to differences in the Sn/Ti ratio of the $Ti_{1-x}Sn_xO_2$ solid solution.

3.4. <u>Used catalysts</u> (JM4, JM6, JM11 and JM12).

The Mössbauer data for the THF insolubles shown on Table X indicate that significant changes occured during the tests. Indeed, in addition to the tin(IV) peak at around zero velocity, due to tin(IV) in a pseudo-octahedral coordination of oxygen, a doublet at high velocity ($\delta \simeq 3.2$mm.s^{-1}) is observed, characteristic of divalent tin with a stereoactive lone pair of electrons. However, the quadrupole splitting is much smaller (about half) than for the non-calcined catalysts ($\Delta \simeq 0.9$mm.s^{-1} instead of $\simeq 1.7$mm.s^{-1}), showing that the tin(II) species that was formed during the test is not surrounded by oxygen. Comparison with the values shown in Table IX reveals that the new divalent tin compound is SnS, stannous sulfide. This is in agreement with the powder X-ray diffraction results which also

showed Bragg peaks due to SnS. Possible traces of beta-Sn suspected by diffraction could not be confirmed by Mössbauer spectroscopy because of the strong overlapping of the beta-Sn and SnS lines. However, if beta-Sn is indeed formed, it can be present only in a small amount. In the case of JM6 (coprecipitated catalyst), the amount of divalent tin is so low that it was not possible to measure the peak positions and therefore to identify the tin(II) species. The amount of tin(II) being very low (<1%) in JM6 confirms the X-ray conclusion that the Bragg peaks observed at about the same position than those of SnS were indeed due to the unidentified crystalline phase already present in the calcined coprecipitated catalyst (JM8) and not to SnS. As outlined before, the sulfur probably originated from the coal used for the test. In agreement with the diffraction results, no sulfide of tin(IV) SnS_2, or mixed oxidation state Sn_2S_3 or Sn_3S_4, is observed, which shows that only divalent tin is sulfided. Mössbauer spectroscopy confirms that no divalent tin survided calcination, such that tin must have been reduced in-situ during the hydroprocessing test, by hydrogen or carbon (reactions I and II) or both. A further proof of this is the result of the tests # 63 and 76, giving respectively the samples JM11 and JM12. In the test # 63, the calcined MB-599 catalyst (JM19) was used, resulting in the THF insoluble JM11 which is found to contain 15% of SnS while in the test # 76, which was carried out using the non-calcined MB-599 catalyst (JM9) the resulting THF insoluble (JM12) contained 10% SnS, when the non-calcined catalyst used for the test (JM9) contained 25% divalent tin. The reason for the difference in SnS content from JM4 (1% Sn) and JM11 (15% SnS), both prepared from a calcined catalyst, probably results from the condition of the test (hydrogen pressure, temperature, time) and the composition of the catalyst Table XII). The decomposition of the $Ti_{1-x}Sn_xO_2$ rutile solid solution to give TiO_2 anatase and SnS, suggested by X-ray diffraction agrees with the Mossbauer results which show that the

catalysts that contain little (or no) $Ti_{1-x}Sn_xO_2$, i.e. JM8 and JM2 give little SnS (i.e. JM8 and JM4 respectively with less than 1% SnS) when the catalyst that is mainly made of $Ti_{1-x}Sn_xO_2$, i.e. JM19, gives 15% SnS (JM11).

The data on Table XII show that all runs were carried out at the same conditions, i.e. at 410°C for 3 hours and 45 minutes, under a hydrogen pressure of 500 psi, therefore changes in the test conditions cannot account for the variation in SnS content. This further reinforces the hypothesis that SnS is formed upon decomposition of the $Ti_{1-x}Sn_xO_2$ solid solution to give TiO_2 anatase and SnS. The difference between JM11 and JM12 (15 and 10% SnS respectively), both tests being carried out at exactly the same conditions, using the same MB-599 catalyst, is probably related to the fact that JM11 was obtained using calcined MB-599 when JM12 was obtained using non-calcined MB-599. The highest yield in SnS for JM11 can also be explained by the fact that, in this case, the calcined catalyst was mainly made of microcrystalline $Ti_{1-x}Sn_xO_2$ as no other phase was detected by X-ray diffraction or Mössbauer spectroscopy, while the non-calcined catalyst did not contain the tin-titanium oxide solid solution. During the test at 410°C, formation of the $Ti_{1-x}Sn_xO_2$ solid solution probably occured, but probably to a lower extend because of the reducing nature of the atmosphere (calcinations were carried out in air, i.e. oxidizing atmosphere), hence formation of a lower amount of SnS (10% instead of 15%).

CONCLUSION

Scanning electron microscopy (SEM), powder X-ray diffraction (XRD) and 119-tin Mössbauer spectroscopy (MS) have been used to characterize tin-supported hydrous titanate catalysts which were prepared at CANMET, Department of Energy, Mines and Resources, and tested for the hydroprocessing of mixtures of heavy oil and coal. Although the tin supported catalysts turned out to be not efficient for coal liquefaction (8), they provide a good model for the structure of other metal supported titanates catalysts, which are efficient catalysts, and their behaviour under reducing conditions in the presence of sulphur. Indeed, while all catalysts could be examined by electron microscopy and powder X-ray diffraction, only the tin catalysts also offered the benefits of a suitable Mössbauer isotope (^{119}Sn) which allows direct probing of the metallic site. This is further reinforced by the low crystallinity of the catalysts which precludes an in-depth study by diffraction techniques. The combination of the three techniques provides a unique opportunity to study the macroscopic structure of the catalysts, i.e. the particle shape and size (using SEM), the long range periodicity in the crystalline phases and identification of these phases (using XRD), and the study of the metal site with determination of oxidation state and phase analysis for both crystalline and non-crystalline phases (using MS). Each of the techniques corroborates the results of the two others and supplies supplementary results such that the information obtained is more complete and allows a more accurate interpretation.

All ion-exchanged catalysts exhibit a low degree of crystallinity with a crystallite size of c.a. 50-300Å diameter, which are loosely packed in structureless agglomerates of various sizes, mostly in the range 1-60μm. All phases observed by X-ray diffraction are microcrystalline and based on TiO_2 and SnO_2, the most common phases being TiO_2 anatase and rutile and SnO_2 rutile. A solid solution, $Ti_{1-x}Sn_xO_2$, in the rutile form, has also been

of crystallinity and are also made of very small agglomerates with no internal structure. A large amount of the divalent tin used for ion exchange is oxidized to tin(IV) in the ion-exchange process. However this can be reduced if the water solvent is degassed to remove dissolved oxygen prior to dissolving $SnCl_2.2H_2O$ and if the solution is kept strongly acidic.

Calcination of the catalysts in air results in oxidation of all the remaining tin(II) to tin(IV). In addition slight sintering occurs as more of larger, but still loose, agglomerates are observed in electron microscopy. Loss of water also occurs, together with growth of the crystallites from <50Å to c.a. 100Å for the tin oxide and 300Å for the titanium oxide. Therefore the catalysts are still microcrystalline.

During the hydroprocessing tests, there seems to be no further sintering. The main change is the formation of SnS in variable quantities. This has been attributed to the sulfur present in coal and seems to be associated with the reduction of a part of tin(IV) to tin(II) in the reducing reaction medium (carbon and pressurized hydrogen). In addition, formation of SnS seem to result from the decompostion the $Ti_{1-x}Sn_xO_2$ solid solution, giving TiO_2 in the anatase form and SnS. Tin(IV) and titanium does not give evidence of sulfidation. The formation of SnS in the conditions of the tests shows that the other metal supported catalysts (Mo, Co, and Ni) must also have resulted in the formation of the corresponding sulfide.

Although the tin catalysts are not efficient, they provided a good model for an in-depth study of these supported catalysts at two stages of their preparation and after use.

RECOMMENDATIONS

The tin supported catalysts are microcrystalline. As a large surface area is probably a necessary condition for high catalytic activity, particle size as small as possible are highly recommended. This goal was well achieved here. Calcination, which often results in crystal growth and sintering, should be avoided whenever possible. Too small particles, although desirable for high activity, have the disadvantage to preclude a detailed diffraction analysis and therefore make identification of the phases present in the material more difficult.

Preparation of the catalysts results in the oxidation of a large amount of tin(II) to tin(IV). The use of degassed water and a strongly acidic pH reduces this undesirable phenomenon from 90-95% to 75%. However, there is still considerable oxidation. This should be more drastically reduced by carrying out the dissolution of $SnCl_2.2H_2O$ under a blanket of inert gas (nitrogen or argon) and reduce the pH as low as possible (the value at which the support starts to dissolve is the limit). Calcination to remove adsorbed and hydration water should be carried out under vacuum to prevent oxidation of tin. This would also make it possible to remove all water at a lower temperature, which in return, would further reduce sintering effects. As the water contained in the catalysts may oxidize tin(II) at high temperature, a slightly reducing atmosphere, such us a H_2/N_2 mixture, may be necessary to avoid oxidation of a part of tin(II) to tin(IV) during calcination.

Sulfur may act as a poison to the catalyst. As tin in the form of $Ti_{1-x}Sn_xO_2$ rutile type solid solution is efficient to remove it, an appropriate amount of this solid solution, mixed with other metal ion exchanged catalysts, may prove useful to reduce or even suppress the formation of metal sulfides. Thus, reduced catalyst poisoning should result in increased efficiency and/or lifetime of the catalysts.

Divalent tin, in the non-supported form, has been reported to yield good results (1-3). This may be a better way to prepare efficient catalysts. Indeed, tin(IV) seems to combine with TiO_2 to form $Ti_{1-x}Sn_xO_2$ solid solution and therefore tin becomes a part of the support instead of being the active metal site. Thus, deposition of tin(II) on coal, with no support, is recommended.

Because of differences in their recoil-free fraction, different tin components of a mixture give a Mössbauer spectrum which is the sum of the spectra of each component, unfortunately, the area of each subspectrum is not directly proportional to the actuel composition of the catalyst unless the recoil-free fraction of all tin sites is the same. Large differences occur mainly between the different oxidation states [Sn(IV) gives stronger spectra than Sn(II) or Sn(0)] and different ligands [oxides give stronger spectra than any other ligand]. Although qualitative identification is still valid, as well as trends in mixtures of the same tin species, absolute quantitative compositions are harder to obtain. Two techniques can be used:

1. If each component can be isolated pure, Mössbauer spectra of several known physical mixtures of the components will yield a calibration curve which can be used to determine the real composition of mixtures.

2. If each component cannot be obtained pure, a good approximation (but not exact) of the composition of the mixture can be obtained by recording spectra vs temperature. Fig.16 shows the change of recoil free fraction with temperature, as a function of the rigidity of the solid lattice. Spectra recorded at very low temperature, near the zero-point motion region, give a smaller, but non-zero, error in composition, while a much larger error is obtained at high temperature. The spectrum of each component vanishes as the temperature is increased close to the Debye temperature of each phase. It results that large errors in compostion can occur at room temperature but these can

be minimized at very low temperature. Therefore, variable temperature studies by Mössbauer spectroscopy is highly recommended in order to obtain a better approximation of the relative amount of each tin species in all catalysts.

REFERENCES

1. S. J. Cochran, M. Hatswell, W. Roy Jackson and F.P. Larskins, Fuel 61, 831 (1982).

2. M. Mizumoto, H. Yamashita and S. Matsuda, Ind. Eng. Chem. Prod. Res. Dev. 24, 394 (1985).

3. P.S. Cook and J.D. Cashion, Fuel 65, 146 (1986).

4. J. Monnier and J. F. Kriz, ACS Preprints, Div. of Petroleum Chemsitry 30, 513 (1985).

5. J. Monnier and J.F. Kriz, 10th Candian Symposium on Catalysis, Preprints (1986).

6. R.G. Dosch, H.P. Stephens and F.V. Stohl, U.S. Patent 4,511,455 (1985).

7. H.P. Stephens, R.G. Dosch and F.V. Stohl, Ind, Eng. Chem. Prod. Res. Dev. 24, 15 (1985).

8. J. Monnier, G. Denes, J. Potter and J.F. Kriz, Energy & Fuels, submitted.

9. G. Denes and I. Ioannidis, to be published.

10. P.Z. Hien and V.S. Shpinel, Soviet Physics JETP 17, 268 (1963), [J. Exptl. Theoret. Phys.(U.S.S.R.) 44, 393 (1963)].

11. B.D. Cullity, "Elements of X-ray Diffraction", 2nd edition, Addison-Wesley Publishing Co, Inc., Don Mills, Ontario, pages 192 & 284 (1978).

12. T. Birchall and G. Denes, Can. J. Chem. 62, 591 (1984).

13. E.M. Baggio and T.J. Sonnino, J. Chem. Phys. 52, 3786 (1970).

14. P.S. Cook, J.D. Cashion and P.S. Cassidy, Fuel 64, 1121 (1985).

15. J. Galy, G. Meunier, S. Anderson and A. Astrom, J. Solid State Chem, 13, 142 (1975).

16. I.D. Brown, J. Solid State Chem. 11, 214 (1974).

17. R.J. Gillespie and R.S. Nyholm, Quaterly Reviews, Chem. Soc. 11, 339 (1957).

18. G. Denes, J. Pannetier, J. Lucas and J. Y. LeMarouille, J. Solid State Chem. 30, 335 (1979).

19. T. Birchall, G. Denes, K. Ruebenbauer and J. Pannetier, J. Chem. Soc. (A), Dalton Tr., 1831 (1981).

20. G. Denes, J. Pannetier and J. Lucas, J. Solid State Chem. 33, 1 (1980).

LIST OF TABLES

I. List of samples studied.

II. Some analytical data for the samples investigated.

III. Techniques used to study the samples.

IV. Experimental parameters for Mössbauer runs.

V. Crystallographic data of relevant compounds compiled for phase identification from X-ray powder diffraction patterns.

VI. X-ray powder diffraction results.

VII. Comparison of the Bragg peaks for SnO_2, TiO_2 and $Ti_{1-x}Sn_xO_2$ rutile type phases.

VIII. Particle size of the samples determined from the X-ray powder patterns.

IX. ^{119}Sn Mössbauer parameters of relevant tin compounds compiled for phase identification by Mössbauer spectroscopy.

X. ^{119}Sn Mössbauer spectroscopic data for the samples.

XI. Amount of divalent tin in the ion-exchanged non-calcined catalysts as a function of preparative conditions.

XII. Amount of SnS stannous sulfide in the THF insolubles versus test conditions.

Table I: List of Samples Studied

JM1: MB-587 non-calcined catalyst obtained from the 1st generation support (JM13), after dissolution of the support, by coprecipitation with Sn.

JM2: MB-586 calcined catalyst, obtained by ion exchange (JM7) from the 1st generation support (JM13), then calcination.

JM3: MB-585 calcined catalyst, obtained by ion exchange (JM10) from the first generation support (JM13), then calcination.

JM4: Run #54, with calcined MB-586 catalyst (JM2) obtained by ion exchange (JM7) from the 1st generation support (JM13).

JM6: Run #55, with calcined MB-587 catalyst (JM8) obtained by coprecipitation with Sn (JM1) from the 1st generation support (JM13).

JM7: MB-586 non-calcined catalyst obtained by ion exchange from the 1st generation support (JM13).

JM8: MB-587 calcined catalyst, obtained by coprecipitation with Sn (JM1) from the 1st generation support (JM13), then calcination.

JM9: MB-599 non-calcined catalyst obtained by ion exchange from the 2nd generation support (JM14).

JM10: MB-585 non-calcined catalyst obtained by ion exchange from the 1st generation support (JM13).

JM11: Run #63, with calcined MB-599 catalyst (JM19) obtained by ion exchange (JM9) from the 2nd generation support (JM14).

JM12: Run #76, with non-calcined MB-599 catalyst (JM19) obtained by ion exchange (JM19) from the 2nd generation support (JM14).

JM13: 1st generation support.

JM14: 2nd generation support.

JM15: Calcined 2nd generation support.

JM19: Calcined MB-599 catalyst (JM9) obtained by ion exchange from the 2nd generation support (JM14).

Table II: Some Analytical Data for the Samples Investigated

Catalyst	Oxide or Metal	Anal. Tech. (*)	---- weight % ---- TiO_2 or Ti	SnO_2 or Sn	Na_2O or Na	-- atomic ratios -- Ti/Sn	Na/Sn	Na/Ti
JM1	Oxide	ICAPS	80.65	10.21		14.57		
JM2	Metal	NA	43.2	12.7	1.08	8.18	0.45	0.06
JM2	Oxide	ICAPS	76.92	16.05	0.35	8.82	0.03	0.003
JM3	Metal	NA	48.2	9.00	1.14	12.63	0.63	0.05
JM3	Oxide	ICAPS	80.12	12.91	0.38	11.22	0.03	0.003
JM4	Oxide	ICAPS		1.97				
JM6	Oxide	ICAPS		0.8				
JM7	Oxide	ICAPS	75.11	14.40		9.5		
JM8	Metal	NA	42.4	3.48	3.52	29.67	5.00	0.11
JM8	Oxide	ICAPS	89.82	6.35	0.53	28.50	0.10	0.004
JM9								
JM10								
JM11	Oxide	ICAPS		3.32				
JM12	Oxide	ICAPS		2.45				
JM13								
JM14								
JM15								
JM19	Metal	NA	36.5	16.8	3.86	5.43	1.22	0.22
JM19	Oxide	ICAPS	58.32	33.16	3.59	3.36	0.14	0.04

*: NA = Neutron activation
ICAPS = Inductive coupled argon plasma spectrometry

Note: "Oxide or Metal": Neutron activation results are given in metal weight % while the ICAPS results are given in metal oxide weight %.

Table III: Techniques used to study the samples

Samples	^{119}Sn Mössbauer Spectroscopy	Powder X-ray Diffraction	Scanning Electron Microscopy
JM1	X	X	X
JM2	X	X	X
JM3	X	X	X
JM4	X	X	
JM6	X	X	
JM7	X	X	X
JM8	X	X	X
JM9	X	X	X
JM10	X	X	X
JM11	X	X	
JM12	X	X	
JM13		X	X
JM14		X	X
JM15		X	X
JM19	X	X	

Table IV: Experimental Parameters for Mössbauer Runs

Sample	Color	Holder	sample mass(mg)	mass Sn/cm² (mg)
JM1	yellow	teflon	643	17.2
JM2	pale yellow	Al	237	10.0
JM3	yellow	Al	295	10.0
JM4	black	Al	1,935	10.0
JM6	black	Al	3,132	6.6
JM7	creme	teflon	300	11.4
JM8	light yellow	Al	600	10.0
JM9	light yellow	teflon	300	
JM10	light creme	teflon	600	
JM11	black	Al	1,147	10.0
JM12	black	Al	1,955	10.0
JM19	white	teflon	302	26.3

	------- 8mm/s -------		------ 2.5mm/s ------	
Sample	Time(h:mn)	Baseline	Time(h:mn)	Baseline
JM1	98:50	4,694,000	23:40	936,000
JM2	17:00	1,136,000	20:40	945,000
JM3	26:15	1,744,000	6:00	256,000
JM4	24:00	1,226,000	63:35	2,085,000
JM6	17:00	706,000	8:35	246,000
JM7	98:30	5,752,000	15:00	712,000
JM8	17:30	453,000	12:45	404,000
JM9	19:00	722,000	10:50	500,000
JM10	246:00	8,342,000	9:00	317,000
JM11	27:30	1,404,000	15:10	648,000
JM12	66:35	2,088,000	8:20	280,000
JM19	29:30	1,268,000	16:00	794,000

Table V: Crystallographic Data of Relevant Tin and Titanium compounds

Compound	Ref.	Unit-cell Parameters	C.S.	Space Group	Z	Structural Type
TiO_2	1	a=3.785(12) c=9.514(6)	TE	$I4_1/amd$	2	Anatase
TiO_2	2	a=4.594 c=2.958	TE	$P4_2/mnm$	2	Rutile
TiO_2	3	a=5.456(2) b=9.182(5) c=5.143(3)	OR	Pcab	8	Brookite
TiO_2 (B)	4	a=12.163(5) b=3.735(2) c=6.513(2) β=107.29(5)	MO			closely related to $K_2Ti_4O_9$, Ti_4O_9 sheets
β-TiO_2 high pressure	5	a=4.531 b=5.498 c=4.900	OR	Pbcn		α-PbO_2
$H_2Ti_4O_9.1.2H_2O$	6	a=19.968(4) b=3.746(1) c=12.025(2) β=114.01(1)	MO	C2/m	4	Layered
$H_2Ti_4O_9.H_2O$	7	a=18.77 b=3.750 c=11.62 β=104.6	MO			Layered
$H_2Ti_3O_7$	7	a=8.080 b=3.752 c=9.178 β=101.27	MO			Layered
$H_2Ti_8O_{17}$	7	a=15.31 b=3.744 c=12.47 β=96.7	MO			Layered
$Na_{0.98}H_{1.02}Ti_4O_9.3.3H2O$	8	a=24.337(5) b=3.763(1) c=12.078(3) β=112.52(2)	MO			Layered

Table V: (continued 1)

Compound	Ref.	Unit-Cell Parameters	C.S.	Space Group	Z	Structural Type
$NaTi_2O_5H$	9					Amorphous
$Na_{1.4}H_{0.6}Ti_4O_9.3.3H_2O$	8	a=24.378(4) b=3.781(1) c=12.054(3) β=113.10(1)	MO			Layered
$NaHTi_4O_9.H_2O$	8					
$Na_2TiO_4.H_2O$	10	a=5.92 c=30.16	TE			
$Na_2Ti_6O_{13}$	11	a=15.131 b=3.745 c=9.159 β=99.30	MO			Rectangular Tunnels
$Na_2Ti_9O_{19}$	12	a=12.2 b=3.78 c=15.3 β=98	MO	C2/m or C2		bronze Type Units
$Na_2Ti_4O_9$	13	a=17.38(2) b=3.784(2) c=11.99(1) β=106.2(1)	MO			Layered
$Na_2Ti_3O_7$	14 15	a=8.576 b=3.801 c=9.143 β=101.60	MO	$P2_1/m$		Layered
$Na_2Ti_7O_{15}$	16					
$NaTiO_2$	17	a=3.02 c=16.2	HE TL	R3m		
Na_2TiO_3	18					
TiS_2	19 20	a=5.6953(2) c=3.4073(2)	HE	P3m1	1	Layered
SnO_2-I Cassiterite	21	a=4.738(3) c=3.188(3)	TE	$P4_2/mnm$	2	Rutile

Table V: (continued 2)

Compound	Ref.	Unit-Cell Parameters	S.G.	Space Group	Z	Structural Type
SnO_2-II	22	a=4.717(1) b=5.727(1) c=5.214(1)	OR			High Pressure
SnO (black) Romarchite	23	a=3.8029(5) c=4.3882(8)	TE	P4/nmm	2	PbO Layered
SnO (red, stabilized by phosphite)	24	a=5.00(1) b=5.72(1) c=11.12(2)	OR	Pbcn	8	
SnO (also red)	25					
Sn_2O_3	26	a=5.457(4) b=8.179(6) c=3.174(3) α=93.8(2) β=92.3(2) γ=90.0(2)	TC		2	
Sn_3O_4	27	a=4.86(16) b=5.88(14) c=8.20(17) α=93.00(17) β=93.21(21) γ=91.00(24)	TC			
$5SnO.2H_2O$ or $Sn_5O_3(OH)_4$ Hydroromarchite	28 29	a=11.5 b=6.03 c=19.8 α=99.00 β=60.30 γ=88.30	TC			
$3SnO.H_2O$ or $Sn_3O_4H_2$	30 31	a=7.93(1) c=9.13(1)	TE	P4/mnc	4	$Sn_6O_4(OH)_4$ Sn_6O_8 units
Na_2SnO_3	32	a=5.29 b=9.53 c=32.51 β=99.6	MO			
$Na_2SnO_3.3H_2O$ or $Na_2Sn(OH)_6$	33 34	a=5.958 c=14.203	HE	R3	3	$[Sn(OH)_6]^{2-}$ distorted octahedra

Table V: (continued 3)

Compound	Ref.	Unit-cell Parameters	C.S.	Space Group	Z	Structural Type
Na_4SnO_4	35					
$Na_2Sn_2O_5$	36					
$Na_4Sn_4O(OH)_{10}$ or $Na_4[Sn(OH)_3]_2[Sn_2O(OH)_4]$	37	a=15.224(5) b=8.300(2) c=12.760(3) β=104.8(2)	MO	$P2_1/n$	4	$[Sn(OH)_3]^-$ and $[Sn_2O(OH)_4]^{2-}$ Units
$Na_2Sn_2O(OH)_4$	37	a=14.50(2) b=16.65(2) c=5.907(8)	OR	$P2_12_12_1$	8	$[Sn_2O(OH)_4]^{2-}$ Units
SnS_2 Berndtite	38	a=3.64 c=5.78	HE			CdI_2 Type Layered
SnS_2	39	a=3.639 b=5.868	HE	P3m1	1	
β-SnS_2 Berndtite	40	a=3.6486 c=5.8992	HE	P3m1	1	
α-$Sn_{1+x}S_2$	41, 42	High temperature, quenchable				
SnS Herzenbergite	43	a=4.332 b=11.224 c=3.988	OR	Pbnm	4	Distorted NaCl Type Layered
SnS Herzenbergite	44	a=4.328 b=11.190 c=3.978	OR	Pbnm	4	
α-SnS (high T)	41 45	High T pattern, limit of $Sn_{1-x}S$ solid solution, non-quenchable, stable >600°C				
Sn_2S_3 Ottemanite	46	a=8.864 b=14.020 c=3.747	OR	Pnam	4	$Sn^{IV}S_6$ octahedra covalent $Sn^{II}S_3$ units
α-Sn_2S_3 (high T)	41 47	Limit of α-$Sn_{2+x}S_3$ solid solution, stable at 745 - 760°C, non quenchable, high T pattern				

Table V: (continued 4)

Compound	Ref.	Unit-cell Parameters	C.S.	Space Group	Z	Structural Type
β-Sn_2S_3 (high T)	41 48	Limit of β-$Sn_{2+x}S_3$ solid solution, stable at 710 - 745°C, non-quenchable, high T pattern				
γ-Sn_2S_3 (high T)	41 49	stoiciometric limit, non quenchable high T pattern				
$NaSnS_2$	50	a=3.69 c=25.54	HE			
α-Sn (grey)	51	a=6.489	CU	Fd3m	8	diamond
β-Sn (white)	52	a=5.831 c=3.182	TE	I4/amd	4	deformed octahedral

Abbreviations used in Table IV:

C.S.: Crystallographic system:
CU = Cubic TE = Tetragonal OR = Orthorhombic
TL = Trigonal HE = Hexagonal MO = Monoclinic
TC = Triclinic

Z: Number of molecules per unit-cell

Unit-cell parameters are in Å (a, b, c) and degrees (α, β, γ).

References for Table V

1. G. Busca, H. Saussay, O. Saur, J.C. Lavalley and V. Lorenzelli, Applied Catalysis 14, 245 (1985) & ASTM 4- 0477.

2. H.D. Megaw, "Crystal Structures: A Working Approach", W.B. Saunders Co., Toronto (1973); ASTM 4-0551; ASTM 21-1276 & NBS Mono. 25, Sec. 7 (1969).

3. NBS Mono. 25, Sec. 3 (1964) & ASTM 16-617.

References for Table V (continued 1)

4. R. Marchand, L. Brohan and M. Tournoux, Mat. Res. Bull. 15, 1129 (1980).

5. Bendeliani et al., Geochemistry International 3, 387 (1966).

6. T. Sasaki, M. Watanabe, Y. Komatsu and Y. Fujiki, Inorg. Chem. 24, 2265 (1985).

7. H. Izawa, S. Kikkawa and M. Koizumi, J. Phys. Chem. 86, 5023 (1982).

8. T. Sasaki, M. Watanabe, Y. Komatsu and Y. Fujiki, Bull. Chem. Soc. Japan 58, 3500 (1985).

9. H.P. Stephens, R.G. Dosch and F.V. Stohl, Ind. Eng. Chem. Prod. Res. Dev. 24, 15 (1985).

10. Kutolin et al., Russ. J. Inorg. Chem. 11, 1180 (1966) & ASTM 19-1226.

11. S. Anderson and A.D. Wadsley, Acta Cryst. 15, 194 & 201 (1962).

12. Y. Bando, M. Watanabe and Y. Sekikawa, Acta Cryst. B35, 1541 (1979).

13. M. Dion, Y. Piffard and M. Tournoux, J. Inorg. Nucl. Chem. 40, 917 (1978).

14. S. Anderson and A.D. Wadsley, Acta Cryst. 14, 1245 (1961).

15. A. Verbaere and M. Tournoux, Bull. Soc. Chim. France 4, 1238 (1973).

16. A.D. Wadsley and W.G. Mumme, Acta Cryst. B24, 392 (1968).

17. Hagenmuller, Lecerf and Onillon, Comptes Rendus 255, 928 (1962).

18. ASTM 11-291.

19. A. H. Thompson, F.R. Gamble and C.R. Symon, Mat. Res. Bull. 10, 915 (1975).

20. R.R. Chianelli, J.C. Scanlon and A.H. Thompson, Mat. Res. Bull. 10, 1379 (1975).

References for Table V (continued 2)

21. ASTM 5-0467.

22. K. Suito, N. Kawai and Y. Masuda, Mat. Res. Bull. 10, 677 (1975).

23. J. Pannetier and G. Denes, Acta Cryst. B36, 2763 (1980).

24. J.D. Donaldson, W. Moser and W.B. Simpson, J. Chem. Soc., 839 (1961)

25. W. Kwestruo and P.G.H.M. Wromans, J. Inorg. Nucl. Chem. 29, 2187 (1967).

26. G. Murken and M. Tromel, Z. Anorg. Allg. Chem. 397, 117 (1973).

27. F. Lawson, Nature 215, 955 (1967).

28. J.D. Donaldson, Acta Cryst. 14, 65 (1961).

29. R.M. Organ and J.A. Mandarino, Can. Mineral. (abstr.) 10, 916 (1971).

30. R.A. Howie and W. Moser, Nature 219, 372 (1968).

31. R.A. Howie and W. Moser, Amer. Mineral. 58, 552 (1973).

32. Lang, Z. Anorg. Chemie 276, 77 (1954) & ASTM 8-219.

33. ASTM 1-1115.

34. C.O. Bjorling, Arkiv for Kemi, Mineralogi och Geologi 15B, 1 (1941).

35. Claverie et al. Bull. Soc. Chim. France, 244 (1966).

36. Scheler, Z. Chemie 8, 150 (1968) & ASTM 21-1165.

37. H.G.V. Schnering, R. Nesper and H. Pelshenke, Z. Anorg. Allg. Chem. 499, 117 (1983).

38. I. Oftedd, Z. Phys. Chem. Liepzig 134, 301 (1928)

39. ASTM 1-1010.

40. NBS Mono. 25, Sec. 9 (1971) & ASTM 22-951.

References for Table V (continued 3)

41. Moh, Neues Jahrb. Mineral. Abh. 111, 227 (1969) & ASTM 22-953.

42. ASTM 22-950.

43. H. Wiedeneier and F.J. Csillag, Z. Krist. 149, 17 (1979) & ASTM 1-0984.

44. Mosburg et al., U.S. Geol. Surv. Prof. Paper 424C, C-347 (1961).

45. ASTM 22-953.

46. D. Mootz and H. Puhl, Acta Cryst. 23, 471 (1967).

47. ASTM 22-952.

48. ASTM 22-955.

49. ASTM 22-954.

50. Le Blanc et al., Bull. Soc. Chim. France, 87 (1969) & ASTM 22-1403.

51. Swanson and Fuyat, NBS Circular 539, 2, 12 (1953) & ASTM 5-0390.

52. Swanson and Tatge, J. C. Fel. Reports, NBS (1951) & ASTM 4-0673.

Table VI: X-ray Powder Diffraction Results

Abbreviations: ? = assignment is tentative or could not be done
* = could be background fluctuations
D = diffuse peak

Notes: $\theta K_\alpha Cu$ = Bragg angle
dhkl(Å) = interplanar spacing
I/Io = relative intensity (in %)
LWHH(°) = linewidth at half height

Alpha-SnF_2 (θ=15.52, LWHH=0.17) was used as reference material for line position and linewidth.

1. JM1: MB-587 non-calcined (coprecipitated from the 1st generation support).

	$\theta K_\alpha Cu$(°)	dhkl(Å)	I/Io	LWHH(°)	Assignment
	11.58	3.840	28	0.20	?
	15.92	2.810	17	0.20	(0 2 -1) Sn_3O_4 ? (-1 1 2) $Sn_5O_3(OH)_4$?
	16.40	2.730	100	0.17	(0 2 1) Sn_3O_4 ? (0 0 3) Sn_3O_4 ?
	23.50	1.933	16	0.20	$Sn_5O_3(OH)_4$?
*	26.33	1.738	11	0.20	$Sn_5O_3(OH)_4$?
	29.20	1.580	27	0.19	$Sn_5O_3(OH)_4$?
*	36.65	1.290	6		?
	39.00	1.224	8		?
	48.03	1.036	9		?

Table VI: (continued 1)

2. JM2: MB-586 calcined (ion exchanged from 1st generation support).

	θK_{α} Cu(°)	dhkl(Å)	I/I0	LWHH(°)	Assignment
	12.70	3 519	100	0.32	(101) TiO_2 anatase
	13.32	3.358	41		(110) SnO_2 rutile
	13.60	3.290	42		(110) $Ti_{1-x}Sn_xO_2$ rutile
	17.78	2.533	15		(101) $Ti_{1-x}Sn_xO_2$ rutile
*	18.15	2.483	9		(101) TiO_2 rutile
	18.98	2.379	19		(004) TiO_2 anatase (200) SnO_2 rutile
	24.00	1.902	32	0.35	(200) TiO_2 anatase
	26.97	1.706	54		(105) TiO_2 anatase
*	27.15	1.695	43		(211) TiO_2 rutile
	27.45	1.678	43		(211) TiO_2 anatase (220) SnO_2 rutile
	28.20	1.637	16		(220) TiO_2 rutile
	31.35	1.487	19		(204) TiO_2 anatase
	37.45	1.272	11		(215) TiO_2 anatase
	41.35	1.171	11		(224) TiO_2 rutile

Table VI (continued 2)

3. JM3: MB-585 calcined (ion exchanged from the 1st generation support).

	θK_{α} Cu(°)	dhkl(Å)	I/Io	LWHH(°)	Assignment
	12.65	3.520	100	0.30	(101) TiO_2 anatase
	13.55	3.290	27	0.70	(110) $Ti_{1-x}Sn_xO_2$ rutile
D	17.00	2.637	9		(101) SnO_2 rutile
	17.75	2.529	21		(101) $Ti_{1-x}Sn_xO_2$ rutile
	18.95	2.374	34		(004) TiO_2 anatase
	19.40	2.321	35		(112) TiO_2 anatase (111) $Ti_{1-x}Sn_xO_2$ rutile
	19.75	2.281	22		(200) TiO_2 rutile
	20.55	2.196	15		(211) TiO_2 rutile
	24.00	1.895	33	0.30	(200) TiO_2 anatase
	26.98	1.694	38		(105) TiO_2 anatase (211) TiO_2 rutile
	27.50	1.670	30		(211) TiO_2 anatase
	31.30	1.484	13		(204) TiO_2 anatase

Table VI (continued 3)

4. JM4: Run # 54 with MB-586 calcined (ion exchanged from first generation support).

	$\theta K_{\alpha}Cu(^{0})$	dhkl(Å)	I/Io	LWHH(^{0})	Assignment
	12.70	3.506	100	0.52	(101) TiO_2 anatase
	13.05	3.414	43		(120) SnS
	13.38	3.331	65		(110) SnO_2 rutile
D	13.70	3.255	30		(110) $Ti_{1-x}Sn_xO_2$ rutile
*	15.25	2.931	17		(200) beta-Sn (101) SnS
	15.85	2.823	21		(111), (130) & (040) SnS (101) beta-Sn
	17.65	2.452	17		(101) $Ti_{1-x}Sn_xO_2$ rutile
	19.05	2.362	17		(004) TiO_2 anatase
D	19.50	2.309	8		(131) SnS
	24.00	1.895	17		(200) TiO_2 anatase
	26.95	1.701	26		(105) TiO_2 anatase (211) TiO_2 rutile
	27.50	1.670	13		(211) TiO_2 anatase (220) SnO_2 rutile
	31.20	1.488	13		(204) TiO_2 anatase

Table VI (continued 4)

5. JM6: Run # 55, with MB-587 calcined (coprecipitated from first generation support).

$\theta K_{\alpha}Cu(^{o})$	dhkl(Å)	I/Io	LWHH(^{o})	Assignment
				$Sn_5O_3(OH)_4$?
12.53	3.553	100	0.65	(120) TiO_2 brookite (101) TiO_2 anatase
12.89	3.456	85		(111) TiO_2 brookite
13.18	3.381	62		(120) SnS (110) SnO_2 rutile
* 13.60	3.278	15		(110) $Ti_{1-x}Sn_xO_2$ rutile
* 13.75	3.278	15		(021) SnS
* 14.25	3.132	10		?
* 14.70	3.038	15		?
* 15.25	2.931	19		(200) beta-Sn (101) SnS
* 15.50	2.885	24		(121) TiO_2 brookite
				$Sn_5O_3(OH)_4$?
15.77	2.836	68	0.20	(111), (130) & (040) SnS (101) beta-Sn
18.75	2.398	12		(201) TiO_2 brookite
19.00	2.368	15		(131) TiO_2 brookite (004) TiO_2 anatase (200) SnO_2 rutile (211)&(220) TiO_2 brookite
22.60	2.006	22	0.18	(150) SnS (211) beta-Sn
23.80	1.941	16		(200) TiO_2 anatase
26.90	1.704	19		(105) TiO_2 anatase
27.35	1.678	16		(211) TiO_2 rutile (211) TiO_2 anatase
31.00	1.496	15	0.55	(204) TiO_2 anatase

Table VI (continued 5)

6. JM7: MB-586 non-calcined (ion exchanged from first generation support).

$\theta K_\alpha Cu(^o)$	dhkl(Å)	I/Io	LWHH(°)	Assignment
13.33	3.344	100	very broad	(110) SnO_2 rutile
17.05	2.269	90	very broad	(101) SnO_2 rutile
25.90	1.765	60	very broad	(211) SnO_2 rutile

7. JM8: MB-587 calcined (coprecipitated from first generation support).

$\theta K_\alpha Cu(^o)$	dhkl(Å)	I/Io	LWHH(°)	Assignment
12.68	3.512	100	0.55	$Sn_5O_3(OH)_4$ & Sn_3O_4 (101) TiO_2 anatase
15.87	2.819	35	0.20	$Sn_5O_3(OH)_4$
18.40	2.442	14		(103) TiO_2 anatase
18.85	2.386	32		(004) TiO_2 anatase
19.15	2.350	23		(112) TiO_2 anatase
22.70	1.998	16	0.26	$Sn_5O_3(OH)_4$
24.00	1.895	35	0.65	(200) TiO_2 anatase
26.95	1.701	30		(105) TiO_2 anatase
27.65	1.661	27		(211) TiO_2 anatase
31.25	1.486	16	0.56	(204) TiO_2 anatase $Sn_5O_3(OH)_4$
37.50	1.265	14	0.58	(215) TiO_2 anatase

Table VI (continued 8)

8. JM9: MB-599 non-calcined (ion exchanged from second generation support).

No defined Bragg peak is observed. Only two broad scattering bands are visible from ca. 12 to 17°(θ) and at ca. 26°(θ), probably due to TiO_2 and SnO_2.

9. JM10: MB-585 non-calcined: (ion exchanged from first generation support).

$\theta K_\alpha Cu(^\circ)$	dhkl(Å)	I/Io	LWHH(°)	Assignment
13.30	3.351	100	very broad	(110) SnO_2 rutile
17.15	2.614	70	very broad	(101) SnO_2 rutile

Table VI (continued 7)

10. JM11: Run # 63 with calcined MB-599 (ion exchanged from second generation support).

	$\theta K_{\alpha}Cu(^{o})$	dhkl(Å)	I/Io	LWHH(^{o})	Assignment
	12.75	3.493	82		(101) TiO_2 anatase
	13.05	3.414	59		(120) SnS
	13.60	3.278	100		(110) $Ti_{1-x}Sn_xO_2$ rutile (021) SnS
	15.25	2.931	36		(200) beta-Sn (101) SnS
	15.85	2.823	64		(111), (040) & (130) SnS (101) beta-Sn
	17.60	2.549	55	0.80	(101) $Ti_{1-x}Sn_xO_2$ rutile
D	19.20	2.344	27		(004) TiO_2 anatase (200) $Ti_{1-x}Sn_xO_2$ rutile (112) TiO_2 anatase (131) SnS
*	22.50	2.014	18		(211) beta-Sn
	24.05	1.892	27		(200) TiO_2 anatase
	26.70	1.716	55		(211) $Ti_{1-x}Sn_xO_2$ rutile (105) TiO_2 anatase
	27.70	1.658	36		(220) $Ti_{1-x}Sn_xO_2$ rutile (211) TiO_2 anatase

Table VI (Continued 8)

11. JM12: Run # 76 with calcined MB-599 (ion exchanged from second generation support).

	θK$_\alpha$Cu(°)	dhkl(Å)	I/Io	LWHH(°)	Assignment
	12.64	3.523	100	0.30	(101) TiO_2 anatase
	13.00	3.427	53		(102) SnS
	13.30	3.351	65		(110) SnO_2 rutile
	13.65	3.267	71		(110) $Ti_{1-x}Sn_xO_2$ rutile (021) SnS
D	15.20	2.940	18		(200) beta-Sn (101) SnS
	15.78	2.835	41		(130) & (111) SnS
	15.98	2.800	35		(040) SnS (101) beta-Sn
*	17.60	2.549	24	0.50	(101) $Ti_{1-x}Sn_xO_2$ rutile
	18.92	2.377	17		(200) TiO_2 rutile
	19.55	2.304	21		(112) TiO_2 anatase (131) SnS (200) $Ti_{1-x}Sn_xO_2$ rutile
	24.02	1.894	25		(200) TiO_2 anatase
*	26.80	1.710	32	0.80	(105) TiO_2 anatase
*	27.45	1.672	24		(220) SnO_2 rutile
*	31.30	1.484	24		(112) beta-Sn (204) TiO_2 anatase

12. JM13: First generation support.
No Bragg is present.

Table VI (Continued 9)

13. JM14: second generation support.
No Bragg peak is observed.

14. JM15: second generation support, calcined.
No Bragg peak is observed.

15. JM19: MB-599 calcined (ion exchanged from second generation support).

$\theta K_{\alpha}Cu(^{o})$	dhkl(Å)	I/Io	LWHH(^{o})	Assignment
13.58	3.283	100	0.70	(110) $Ti_{1-x}Sn_xO_2$ rutile
17.40	2.578	63	1.05	(101) $Ti_{1-x}Sn_xO_2$ rutile
19.30	2.332	13		(200) $Ti_{1-x}Sn_xO_2$ rutile
20.40	2.212	16		(111) $Ti_{1-x}Sn_xO_2$ rutile
26.60	1.722	53		(211) $Ti_{1-x}Sn_xO_2$ rutile
27.60	1.664	25		(220) $Ti_{1-x}Sn_xO_2$ rutile

Table VII: Comparison of the Bragg peaks for SnO_2, TiO_2 and $Ti_{1-x}Sn_xO_2$ rutile type phases

		Bragg angles Theta (°)					
hkl	I/Io	SnO_2	$Ti_{1-x}Sn_xO_2$	TiO_2	JM19	JM2	JM3
110	100	13.32	13.58	13.72	13.58	13.60	13.55
101	90	17.06	17.40	18.06	17.40	17.78	17.75
200	23	19.01	19.39	19.61	19.30		19.45
111	5	19.51	20.00	20.63	20.40		
211	80	25.90	26.54	27.18	26.60		
220	19	27.40	28.01	28.34	27.60	28.20	

NOTE:
The peaks for the solid solution were calculated from the two first peaks of JM19. The peaks for SnO_2 and TiO_2 are given for comparison.

Table VIII: Particle sizes determined from powder X-ray diffraction

Sample	$\theta K_\alpha Cu(^0)$	$B_M(^0)$	$B_S(^0)$	$B(^0)$	t(Å)	Compound
	11.58	0.20	0.18	0.09	931	?
JM1	15.92	0.20	0.18	0.09	948	?
	16.40	0.17	0.18	0.00	>1,000	?
JM2	12.70	0.32	0.17	0.27	301	TiO_2 anatase
JM3	12.65	0.30	0.17	0.25	330	TiO_2 anatase
	13.55	0.70	0.17	0.68	120	SnO_2 rutile
						TiO_2 rutile
JM4	12.70	0.52	0.18	0.49	167	TiO_2 anatase
	peak overlapping, width cannot be measured					TiO_2 brookite
						TiO_2 anatase
JM6	15.77	0.20	0.17	0.11	784	SnS
						beta-Sn
	22.60	0.18	0.17	0.06	1,456	SnS
						beta-Sn
JM7	very broad peak, width cannot be measured				50-100	TiO_2 micro.
						SnO_2 micro.
JM8	15.87	0.20	0.17	0.11	785	?
	24.00	0.65	0.17	0.63	139	TiO_2 anatase
JM9	very broad peak, width cannot be measured				50-100	TiO_2 micro.
						SnO_2 micro.
JM10	very broad peak, width cannot be measured				50-100	TiO_2 micro.
						SnO_2 micro.
JM11	17.60	0.80	0.17	0.78	107	$Ti_{1-x}Sn_xO_2$
JM12	12.64	0.30	0.17	0.25	330	TiO_2 anatase
	17.60	0.50	0.17	0.47	177	$Ti_{1-x}Sn_xO_2$
JM13	no Bragg peak observed				<50	micro.
JM14	no Bragg peak observed				<50	micro.
JM15	no Bragg peak observed				<50	micro.
JM19	13.58	0.70	0.17	0.68	120	$Ti_{1-x}Sn_xO_2$
	17.40	1.05	0.17	1.04	80	$Ti_{1-x}Sn_xO_2$

Table VIII (continued)

Notes: "micro." means "microcrystalline phase".

The average particle t(Å) was taken from the Scherrer formula

$$t = (0.9\lambda)/(B.\cos\theta)$$

where t is the average particle size in Å
λ is the wavelength of the radiation in Å
θ is the Bragg angle for the Bragg peak used
B is the broadening at half height due to the small dimension of the particles

and correction for instrumental line broadening was done using Warren's method:

$$B^2 = B_M^2 - B_S^2$$

where B_M is the experimental linewidth for the sample
B_S is the experimental linewidth for a well crystalline standard material (particle diameter > 1,000Å)

Table IX: ^{119}Sn Mössbauer Parameters of Standards and Relevant Related Tin Compounds

Compound	Ref.	T(°K)	(mm/s)	(mm/s)	Sn Type
SnO_2 cassiterite	1		0.00	0.64(3)	4+
SnO_2 cassiterite	TW	298	0.00(1)	0.60(1)	4+
SnO black	2	NS	2.71	1.45	2+
SnO black	3	295	2.70	1.27	2+
SnO black	TW	298	2.695(4)	1.235(8)	2+
SnO red stabilized with phosphite	2	NS	2.60	2.20	2+
Sn_2O_3	4	RT	0.02(2)	0.56(4)	4+
			2.59(2)	1.96(4)	2+
$Sn_5O_3(OH)_4$	2	NS	2.85	2.04	2+
$SnO.yH_2O$	5	RT	2.92(11)	2.06(8)	2+
$SnO_2.xH_2O$ in tin-treated coal	5	RT	-0.01(2)	0.54(3)	4+
$NaSn(OH)_3$	2	NS	2.60	2.29	2+
$Na_2SnO_3.3H_2O$	10	LN	0	NS	4+
$Na_2SnO_3.3H_2O$	TW	298	0.00(1)	0.00(1)	4+
SnS	6	293	3.29(1)	0.87(1)	2+
Sn_2S_3	8	295	3.48	0.95	2+
			1.10	0	4+
Sn_3S_4	9	NS	3.41(5)	1.00(5)	2+
			1.11(5)	NS	4+
SnS_2	7	78	1.060	0	4+
$Sn_3(PO_4)_2$	11	80	3.03	1.6	2+
$Sn(CH_2ClCO_2)_2$	12	80	3.03	1.66	2+
$Sn(CH_3CO_2)_2$	12	80	3.14	1.77	2+
$Sn(HCO_2)_2$	12	80	2.98	1.56	2+

Table IX: (continued 1)

Compound	Ref.	T(°K)	(mm/s)	(mm/s)	Sn Type
$Sn(SO_3NH_2)_2$	12	80	3.22	1.85	2+
SnO/B_2O_3 glass 33.53% mol. SnO	13	80	3.13	1.83	2+
Some SnF_2/MF frozen aqueous solutions (M=alkali metals)	14	80	similar values		2+
$SnHPO_3$	15	80	3.03	1.60	2+
$K_4Sn(HPO_3)_3$	15	80	2.98	1.74	2+
Alpha-Sn (grey)	16	NS	1.93(2)	0	0
Beta-Sn (white)	16	NS	2.55(2)	0.43(2)	0
Alpha-SnF_2	17	295	3.430(3)	1.532(3)	2+
$CaSnO_3$	TW	295	0 (ref.)	0.00(1)	4+

Notes:

1. Alpha-SnF_2 and $CaSnO_3$ were used for calibration and $CaSnO_3$ as reference of isomer shifts ($\delta[CaSnO_3]=0$ at room temperature).

2. When results for the same compounds have been published more than once, we have given here the most recent and/or the most reliable data.

Abbreviations used in Table VI:

δ ($mm.s^{-1}$): isomer shift, relative to $CaSnO_3$ at RT. When literature values are given relative to another reference, conversion to values relative to $CaSnO_3$ has been done using the values given by Greenwood and Gibb (18).

Δ ($mm.s^{-1}$): quadrupole splitting.
TW: this work.
NS: not specified in the quoted reference.
RT: room temperature
LN: liquid nitrogen temperature

References for Table IX

1. E.M. Baggio and T.J. Sonnino, J. Chem. Phys. 52, 3786 (1970).
2. C.G. Davies and J.D. Donaldson, J. Chem. Soc.(A), 946 (1968).
3. B.I. Boltaks, K.V. Perepech, P.P. Seregin and V.T. Shipatov, Inorganic Materials 6, 717 (1970); [Izvestiya Akademii Nauk SSSR, Neorganicheskie Materials 6, 819 (1970)].
4. K. Hasselback, G. Murken and M. Tromel, Z. Anorg. Allg. Chem. 397, 127 (1973).
5. J.K. Flinn, J. Chem. Phys. 48,882 (1968).
6. P.S. Cook, J.D. Cashion and P.J. Cassidy, Fuel 64, 1121 (1985).
7. J.C. Jumas, S. Del Bucchia, E. Philippot and M. Maurin, J. Solid State Chem. 41, 50 (1982).
8. R. H. Herber and R.F. Davis, J. Inorg. Nucl. Chem. 42, 1577 (1980).
9. G. Amthauer, J. Fenner, S. Hafner, W.B. Holzapfel and R. Keller, J. Chem. Phys. 70, 4837 (1979).
10. C.G. Tschakarov, V. Rusanov and G. Gospodinov, J. Solid State Chem. 59, 265 (1985).
11. M. Cordey-Hayes, J. Inorg. Nucl. Chem. 26, 915 (1964).
12. J.E. Cassidy, W. Moser, J.D. Donaldson, A. Jelen and D.G. Nicholson, J. Chem. Soc.(A), 173 (1970).
13. A. Paul, J.D. Donalson, M.T. Donoghue and M.J.K. Thomas, Phys. Chem. Glasses 18, 125 (1977).
14. T. Birchall and G. Denes, Can. J. Chem. 62, 591 (1984).
15. C,G. Davies, J.D. Donaldson and W. Simpson, J. Chem. Soc.(A), 417 (1969).
16. N. N. Greenwood and T. C. Gibb, "Mossbauer spectroscopy", Chapman and Hall Ltd. London, (1971), capter 14.
17. T. Birchall, G. Denes, K. Ruebenbauer and J. Pannetier. J. Chem. Soc., Dalton Tr., 1831 (1981).

Table X: ^{119}Sn Mössbauer spectroscopic results

Sample	δ(mm/s)	Δ(mm/s)	Tin oxidat. state	% contr.	Assignment
	--- +/- 0.01 ---				
JM1	-0.09	0.15	+4	95	Sn/O octa sd
	3.06	1.66	+2	5	Sn(II)/O
JM2	-0.03	0.30	+4	100	Sn/O octa dist
JM3	-0.03	0.15	+4	100	Sn/O octa sd
JM4	-0.03	0.40	+4	99	Sn/O octa vd
	3.16	0.98	+2	1	SnS
JM6	-0.03	0.00	+4	>99	Sn/O octa reg
	too weak to be mesured			<1	Sn(II)/O
JM7	-0.09	0.15	+4	95	Sn/O octa sd
	3.04	1.59	+2	5	Sn(II)/O
JM8	-0.09	0.15	+4	100	Sn/O octa sd
JM9	-0.09	0.40	+4	75	Sn/O octa vd
	3.13	1.78	+2	25	Sn(II)/O
JM10	-0.09	0.15	+4	90	Sn/O octa sd
	2.88	1.90	+2	10	$SnO.yH_2O$
JM11	-0.03	0.00	+4	85	Sn/O octa reg
	3.22	0.86	+2	15	SnS
JM12	-0.03	0.00	+4	90	Sn/O octa reg
	3.28	0.86	+2	10	SnS
JM19	-0.03	0.00	+4	100	Sn/O octa reg

Notes:

1. δ = chemical isomer shift, relative to $CaSnO_3$ at room temperature.
2. Δ = quadrupole splitting.
3. Tin oxidat. state = tin oxidation state.

Table X (continued)

4. % contr. = % contribution of the tin site to the total Mössbauer spectrum.
5. Sn/O octa = tetravalent tin in octahedral site (can be distorted) of oxygen.
6. reg = regular, i.e. non-distorted octahedral site
7. sd = slightly distorted octahedral site.
8. vd = very distorted octahedral site.
9. Sn(II)/O = divalent tin coordinated to oxygen.

Table XI: Amount of divalent tin in ion-exchanged non-calcined catalysts as a function of preparative conditions

Catalyst	Support	water degassing	pH	stirring time(min)	Sn(II)/total Sn
JM7	JM13	No	2.8	60	5
JM9	JM14	Yes	1.83	105	25
JM10	JM13	Yes	2.4	60	10

Table XII: Amount of SnS versus test conditions

JMx	Catalyst	ie/cop	c/nc	Run	pH_2 (psi)	T(°C)	Time	%SnS
JM4	MB-586	ie	c	54	500	410	3h45	1
JM6	MB-587	cop	c	55	500	410	3h45	<1
JM11	MB-599	ie	c	63	500	410	3h45	15
JM12	MB-599	ie	nc	76	500	410	3h45	10

Notes:

1. ie = ion exchanged, cop = coprecipitated
2. c = calcined, nc = non-calcined
3. pH_2 = hydrogen pressure in the reactor for the test.

LIST OF FIGURES

1. Diagram of samples history.

2. SEM micrograph of JM1 (magnification: upper half x 1,000, lower half x 5,000).

3. SEM micrograph of JM2 (magnification: upper half x 1,000, lower half x 10,000).

4. SEM micrograph of JM3 (magnification: upper half x 810, lower half x 8,100).

5. SEM micrograph of JM7 (magnification: upper half x 800, lower half x 8,000).

6. SEM micrograph of JM8 (magnification: upper half x 700, lower half x 7,000)

7. SEM micrograph of JM9 (magnification: upper half x 800, lower half x 8,000).

8. SEM micrograph of JM10 (magnification: upper half x 800, lower half x 8,000).

9. SEM micrograph of JM13 (magnification: x 2,000).

10. SEM micrograph of JM14 (magnification: upper half x 5,000, lower half x 10,000).

11. SEM micrograph of JM15 (magnification: upper half x 990, lower half x 9,900).

12. X-ray powder pattern of the MB-586 catalyst at various stages: (a)= support (JM13), (b)= non-calcined ion-exchanged catalyst (JM7), (c)= calcined catalyst (JM2), (d) = used catalyst in THF insolubles (JM4). The peaks labelled X on pattern (b) could not be identified. The peak labelled X on patterns (c) and (d) is assigned to the (101) peak of $Ti_{1-x}Sn_xO_2$ rutile solid solution (see fig. 13). The interpolated baseline (dashed line) is just a guide for the eye.

13. X-ray powder pattern of the MB-599 catalyst at various stages: (a)= support (JM14), (b)= non-calcined ion exchanged catalyst (JM9), (c)= calcined catalyst (JM19), (d)= used catalyst (using calcined JM19) in THF insolubles of run # 83 (JM11), (e)= used catalyst (using non-calcined JM9) in THF insolubles of run # 76 (JM12). The interpolated baseline (dashed line) is just a guide for the eye.

14. X-ray powder pattern of the MB-585 catalyst at various stages: (a)= support (JM13), (b)= non-calcined ion-exchanged catalyst, (c)= calcined catalyst (JM3). The interpolated baseline (dashed line) is just a guide for the eye.

15. X-ray powder pattern of the MB-587 catalyst: (a)= support (JM13), (b)= non-calcined coprecipitated catalyst (JM1), (c)= calcined catalyst (JM8), (d)= used catalyst in run # 55 (JM6). The interpolated baseline (dashed line) is just a guide for the eye. The peaks labelled X on patterns (b),(c) and (d) could not be identified.

16. Comparison of the evolution of the recoil-free fraction with temperature for soft lattice and hard lattice compounds.
    fa = recoil-free fraction for the absorber (sample).
    TD1, TD2 = Debye temperature of compounds 1 and 2 respectively.
    1 = soft lattice compound (small recoil-free fraction).
    2 = hard lattice compound (high recoil-free fraction).
    E_L, E_H = errors in relative composition of a mixture of compounds 1 and 2, based on their relative contribution to a Mössbauer spectrum, at low and high temperatures respectively, assuming equal recoil free-fractions.

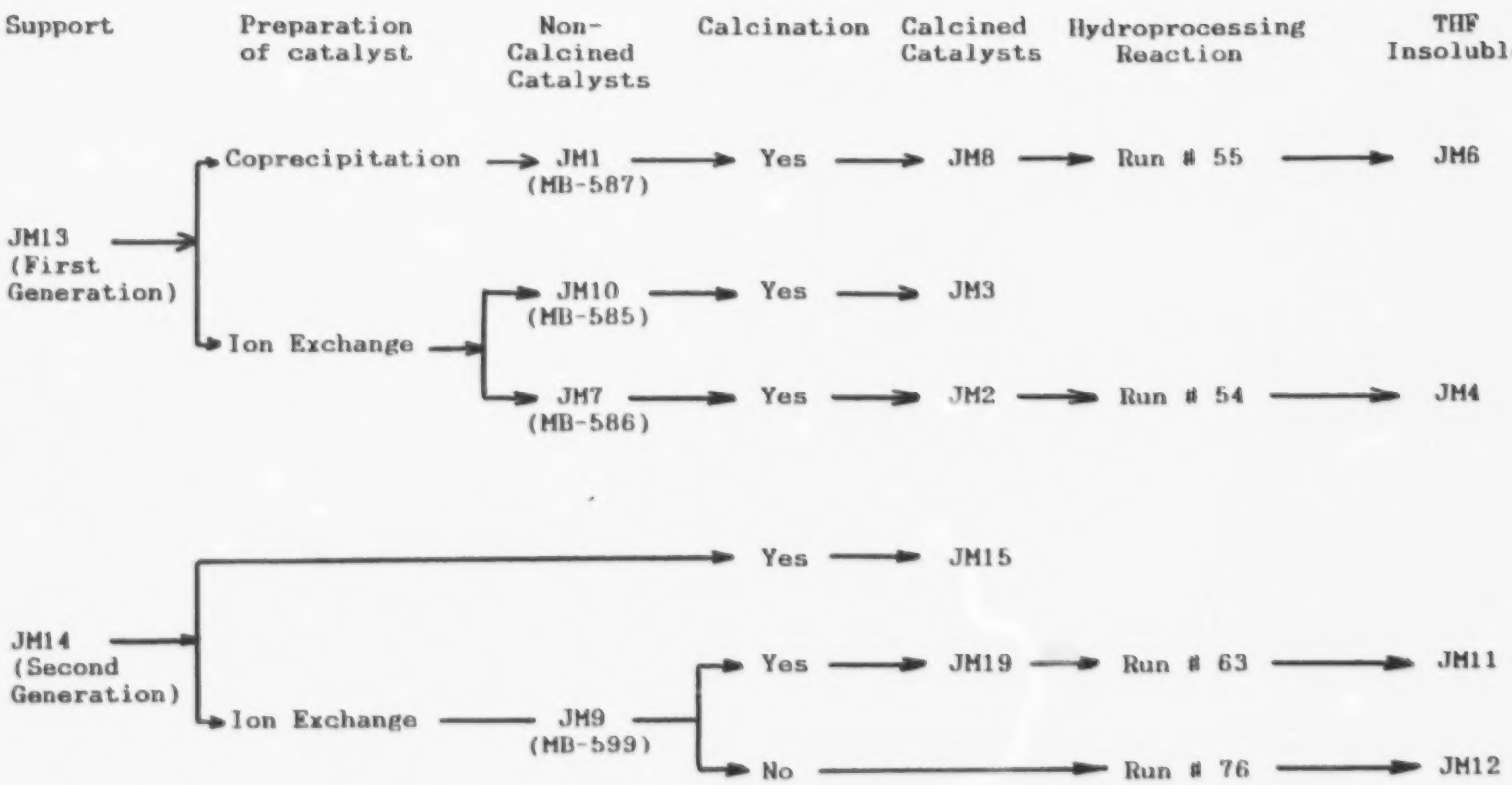

Figure 1: Diagram of sample history

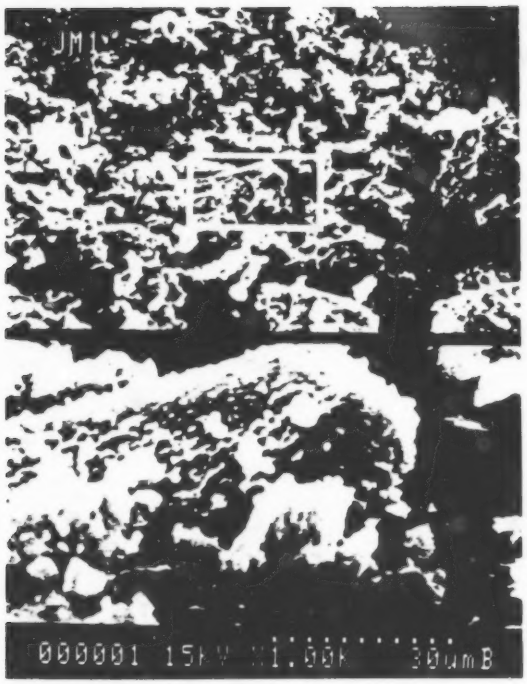

Figure 2: SEM micrograph of JM1
magnification: upper-half: x 1,000
lower-half: x 5,000

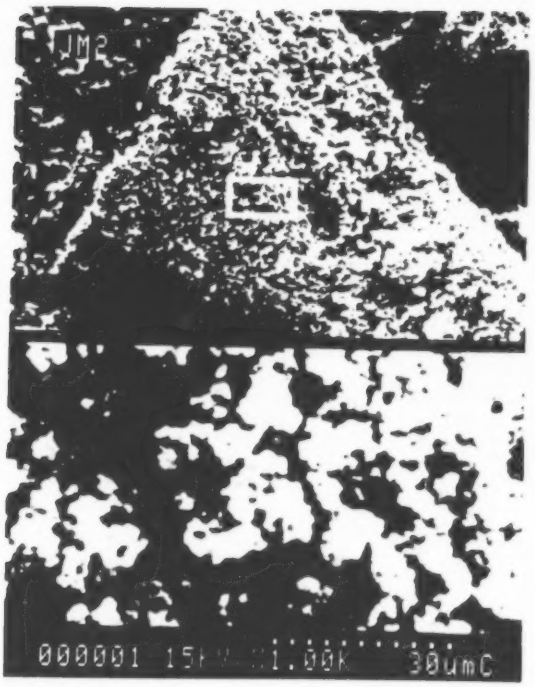

Figure 3: SEM micrograph of JM2
magnification: upper half: x 1,000
lower half: x 10,000

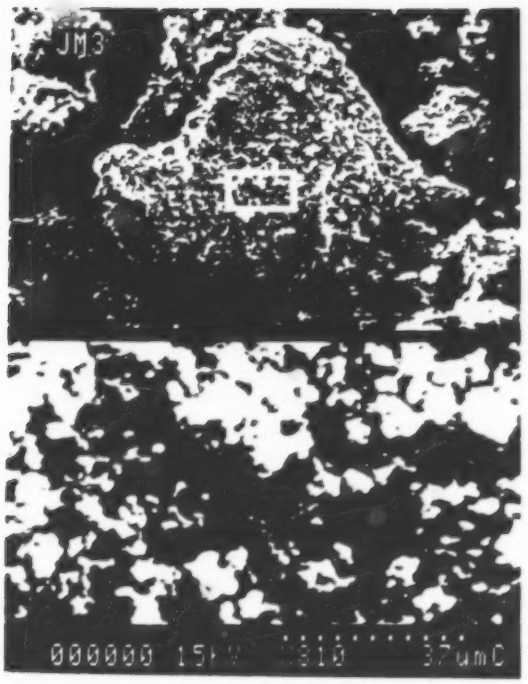

Figure 4: SEM micrograph of JM3
magnification: upper half: x 810
lower half: x 8,100

Figure 5: SEM micrograph of JM7
magnification: upper half: x 800
lower half: x 8,000

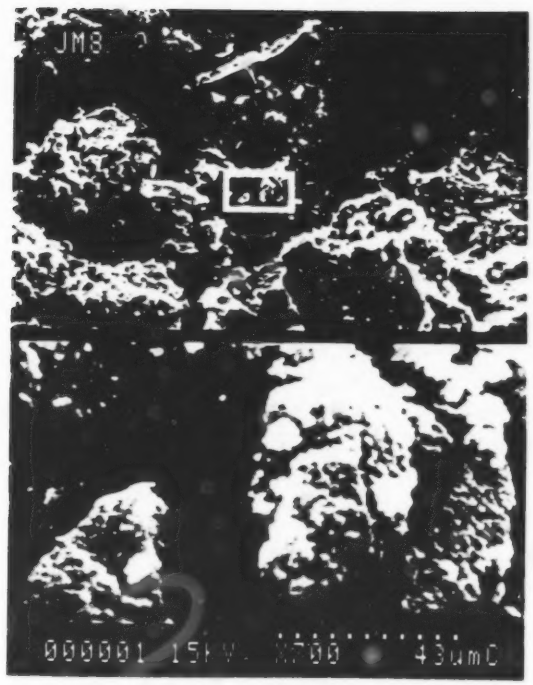

Figure 6: SEM micrograph of JM8
magnification: upper-half: x 700
Lower-half: x 7,000

Figure 7: SEM micrograph of JM9
magnification: upper half: x 800
lower half: x 8,000

Figure 8: SEM micrograph of JM10
magnification: upper half: x 800
lower half: x 8,000

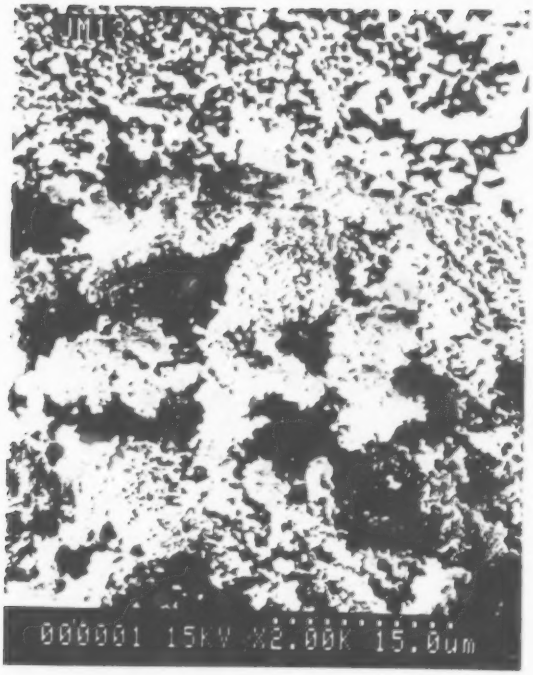

Figure 9: SEM micrograph of JM13
magnification: x 2,000

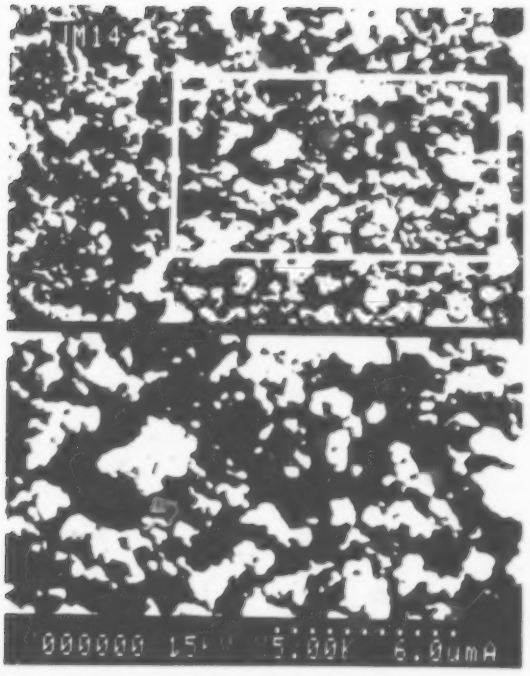

Figure 10: SEM micrograph of JM14
magnification: upper half: x 5,000
lower half: x 10,000

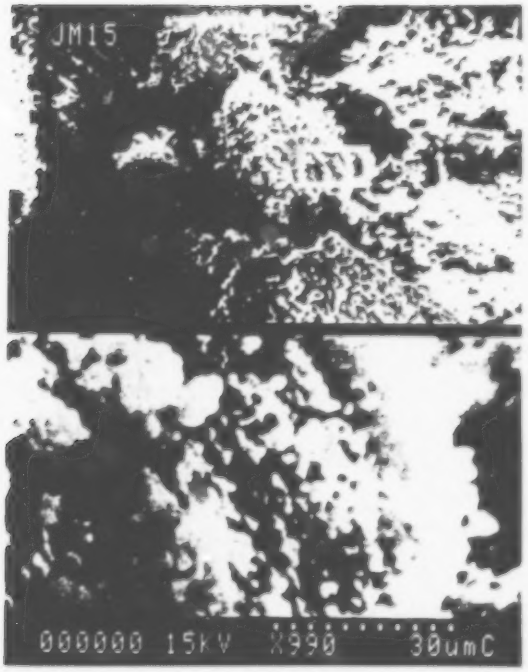

Figure 11: SEM micrograph of JM15
magnification: upper-half: x 990
lower-half: x 9,900

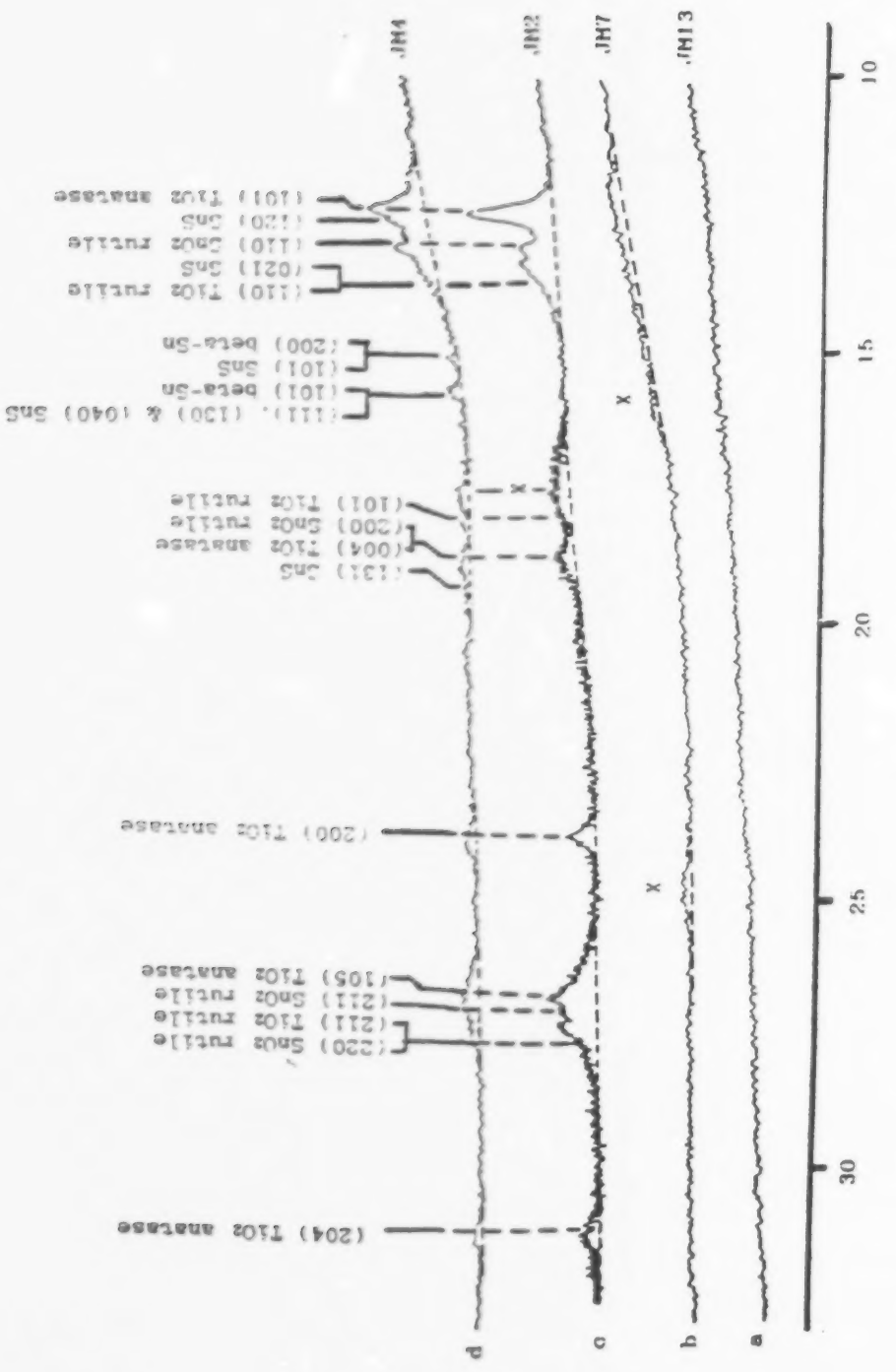

Figure 12: X-ray powder pattern of the MB-586 catalyst.

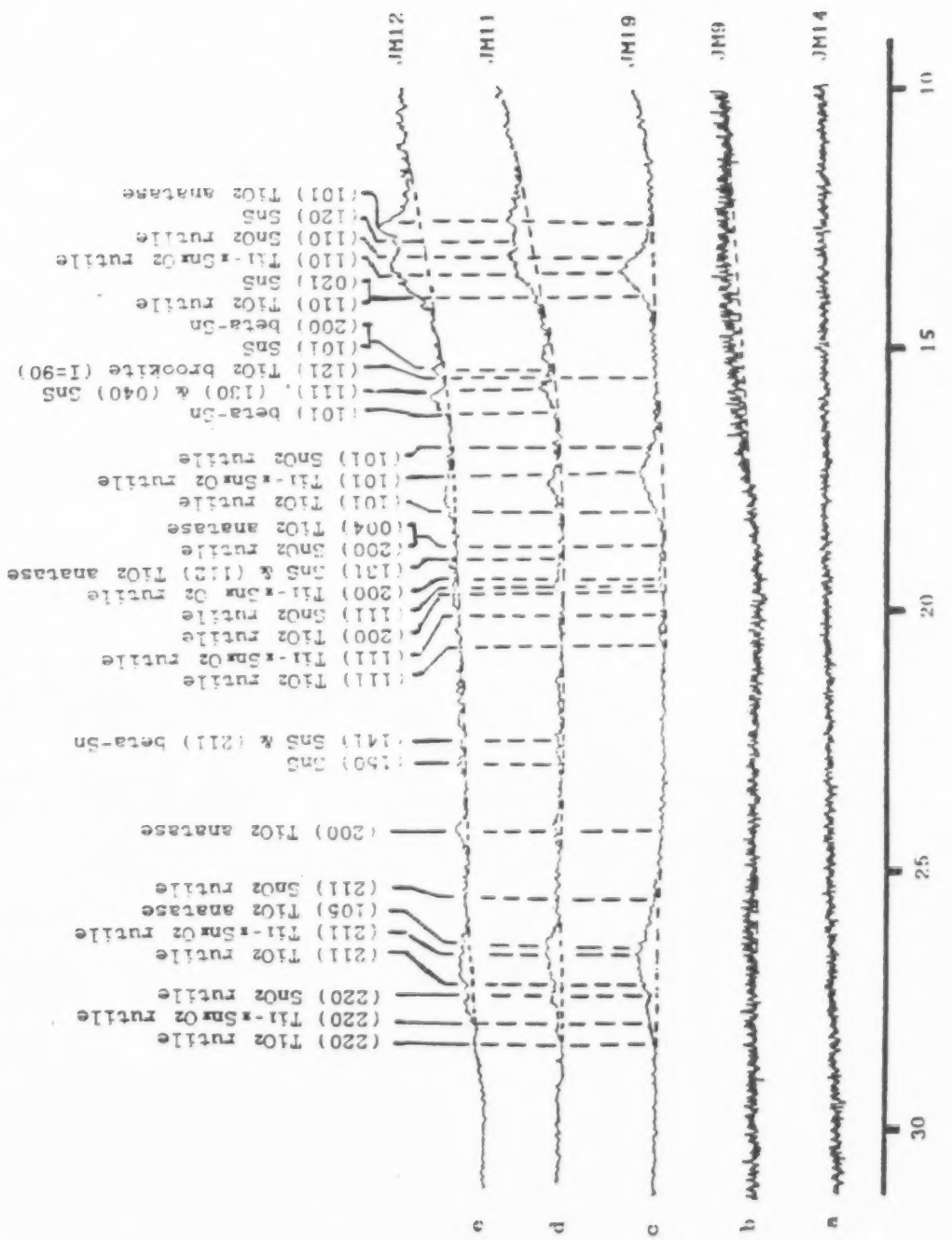

Figure 13: X-ray powder pattern of the MB-599 catalyst

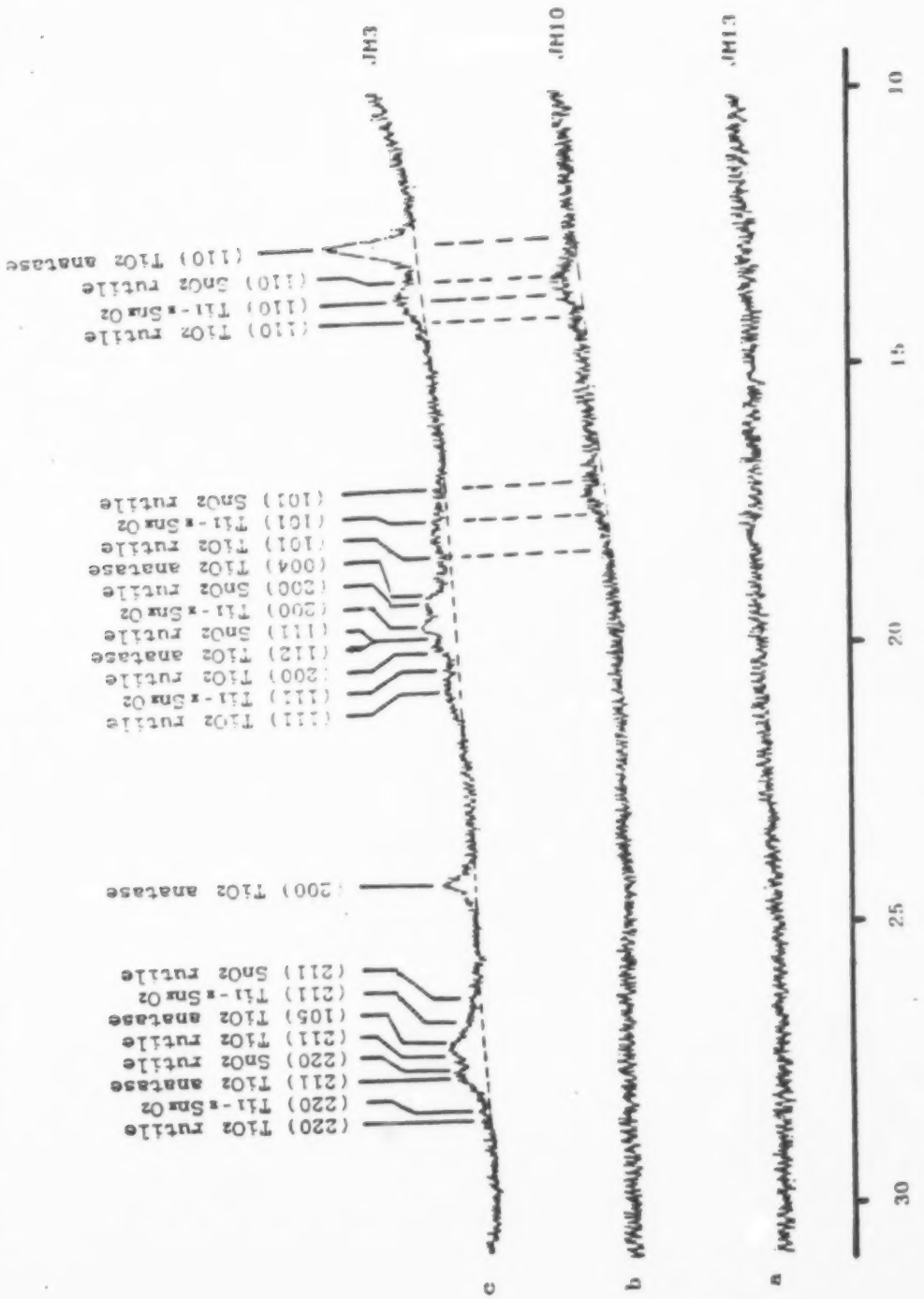

Figure 14: X-ray powder pattern of the MB-585 catalyst

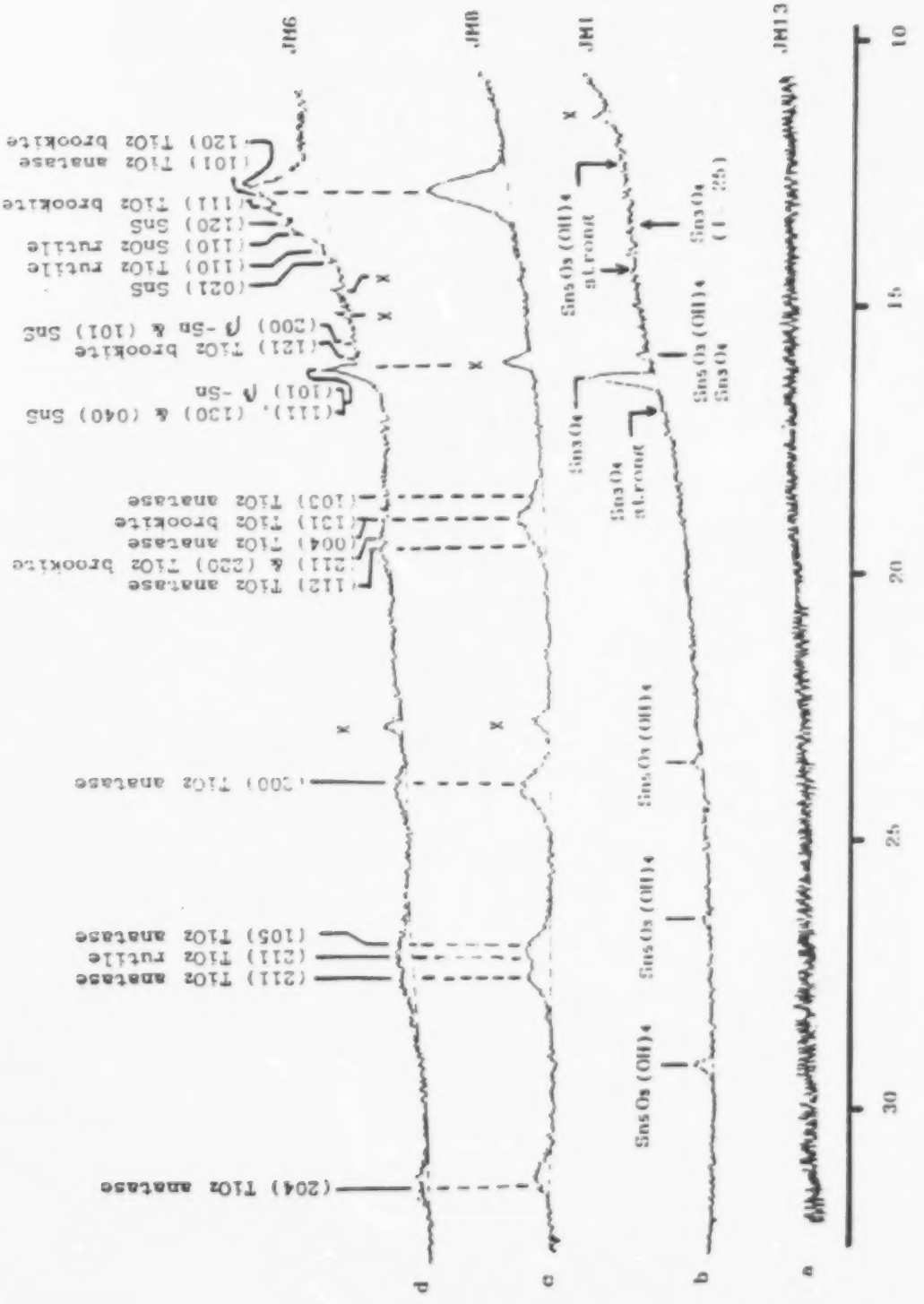

Figure 15: X-ray powder pattern of the MB-587 catalyst.

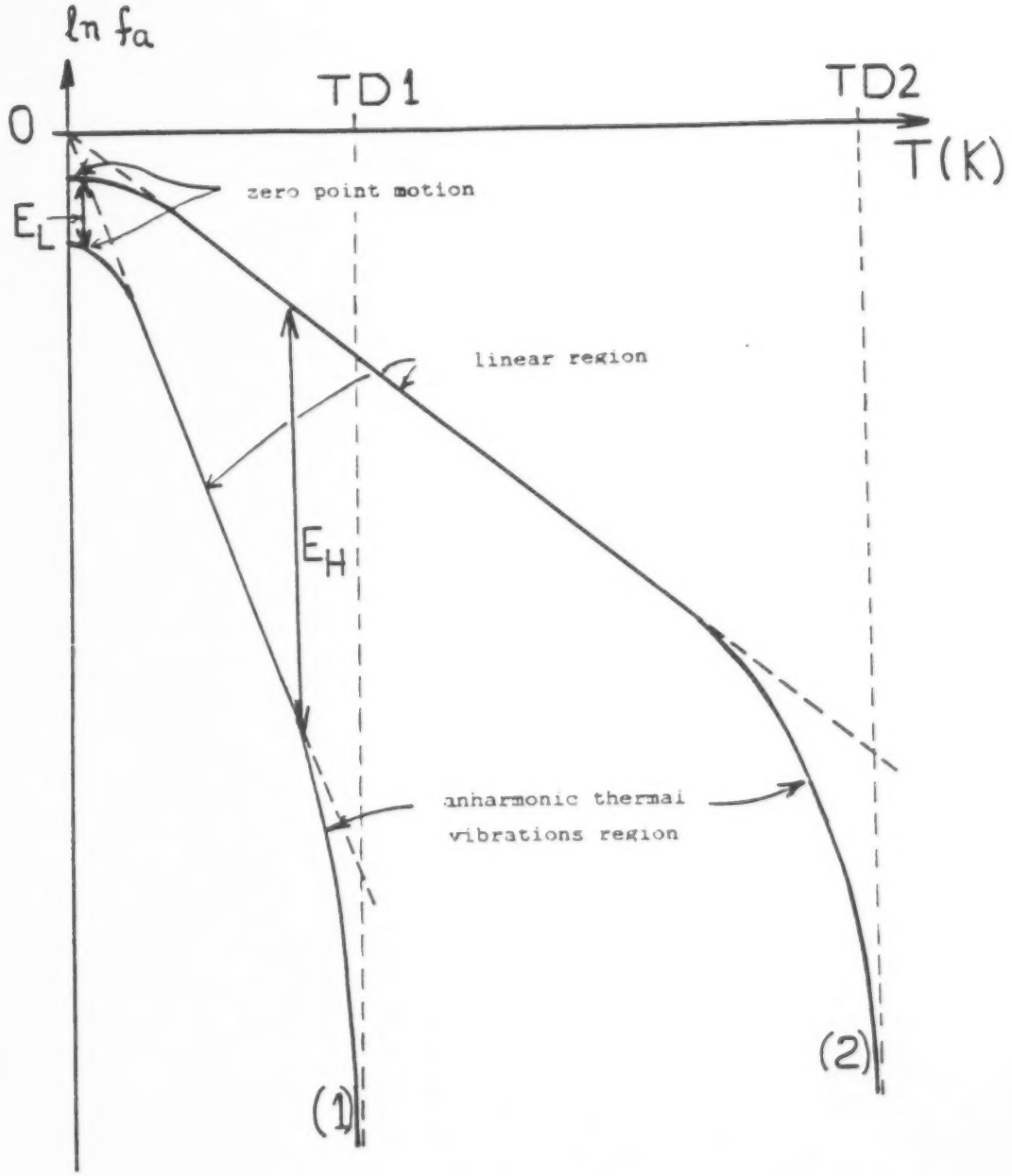

Figure 16: Evolution of the recoil-free fraction with temperature